Integration of synthetic astrocytes into neuroblastoma spheroids *via* droplet based microfluidics

- Master thesis -

Author

Júlia Csatári

Aalborg University
Department of Physics and Nanotechnology

Title:

Integration of synthetic astrocytes into tumour neuronal spheroids *via* droplet based microfluidics

Theme:

Nanobiotechnology

Project Period:

Spring Semester 2019

Project Group:

-

Participant(s):

Júlia Csatári

Supervisor(s):

Oskar Staufer

Leonid Gurevich

Copies: 1

Page Numbers: 70

Date of Completion:

June 10, 2019

Abstract:

To accurately mimic tissues with high accuracy *in vitro*, 3D cell culture-models termed spheroids are receiving increased attention in research. Using microfluidic methods to form spheroids can offer a well-defined microenvironment for controlled assembly, where the cell-cell distance is reduced, boosting intercellular interactions. Here, we present and assess a microfluidic scaffold-free approach for high throughput neuroblastoma-astrocyte co-culture spheroids and neuroblastoma-giant unilamellar vesicle semi-synthetic spheroid formation. After successful generation of neuronal spheroids, differentiation dynamics into mature neuronal networks are assessed under three conditions: 1) Treatment with retinoic acid (a potent inducer of neuronal differentiation), 2) defined co-culture with astrocytes and 3) a hybrid spheroid of living neurons and minimal synthetic astrocytes harbouring NrCAM adhesion proteins. The generation of the latter will exemplarily demonstrate how minimalistic synthetic cells can probe specific differentiation and neuron-glia interaction patterns. For all three approaches, morphological analysis and expression of differentiation markers were evaluated.

Contents

Preface

This master thesis was written as part of the Nanobiotechnology master's program of the Aalborg University. The thesis was conducted at the Department of Cellular Biophysics at the Max Planck Institute for Medical Research, Heidelberg between February 2019 and June 2019.

The author of this thesis is Júlia Csatári, the supervisors are Oskar Staufer and Leonid Gurevich.

Aalborg University, June 10, 2019

Author
<jcsata17@student.aau.dk>

Acknowledgments

Chapter 1

1.Introduction

1.1. Neuronal cell and models to study their mechanisms of function and dysfunction

The brain is an extensively complex organ, which consists of several areas, layers and cell types. Two highly specialized cell types can be accentuated, neurons and glia cells.

Neurons or nerve cells form an interconnected cellular assembly in the central nervous system, acting as fundamental processing units of the brain. The main function of these cells is to receive, convert and produce electric or chemical signals. Understanding these mechanisms is crucial regarding neurophysiology and neuropsychology.

To model neuronal function and behaviour or diseases, transformed neuronal-like cell lines are widely used to overcome the limitations of primary mammalian derived neurons, which once reach maturation via differentiation, are incapable of propagation [1].

Immortalized *SH-SY5Y* cell line is a transformed neuroblastoma cell line derived from malignant tumour. Neuroblastoma is the most common extracranial tumour in children with remarkable clinical heterogeneity [2] . Important attributes to consider are their viability in both non-adherent neuroblastic (N-type) and a (due to selective subcloning) very small population of substrate adherent (S-type) [3] . These properties also influences their feasibility to differentiate them into a more mature neuron-like phenotype. Following differentiation processes, cells can be characterized by neuronal markers and neuronal-like morphology. In the undifferentiated form, *SH-SY5Y* cells are morphologically neuroblast-like, non-polarized cell bodies (which might grow in clusters) with few, truncated processes, and can be characterized by lack of neuronal markers and continuous proliferation [1].

Following differentiation treatment, *SH-SY5Y* cells become morphologically more comparable to primary neurons with distinct, polarized cell bodies and numerous, but randomly distributed, long, exquisite processes. Forster *et al.* showed, that in undifferentiated cell populations, the interconnection between neurons is less than 2%, while over 99% of differentiated cells present this property, which indicates a morphologically defined differentiation efficiency above 97% [4].

With the declining proliferation rate, as cells are withdrawn from the cell cycle, the activity of a neuron specific enolase (NSE) in neuronal and neuroendocrine tissues, the dominant enolase-isoenzyme, is increased [3][1] .

Upon inducing the differentiation in *SH-SY5Y* cells, a variety of adult neuronal phenotypes including cholinergic, adrenergic, or dopaminergic can be modelled, depending on methods and media conditions [1]. This heterogeneity further leverages the potential of *SH-SY5Y* cells for screening in neuroscience and makes the cell line a great model for e.g. to Parkinson's and Alzheimer's disease [5, 6] as well as pathogenesis of viral infections [7].

1.1.1. <u>Retinoic acid treatment</u>

It can be stated that fully differentiated *SH-SY5Y* neurons provide a closer resemblance to mature human neurons found *in vivo* than their undifferentiated counterparts [7]. Retinoic acid treatment is one of the most commonly implemented and best-characterized methods for inducing the differentiation in *SH-SY5Y* cells. Neuroblastoma cell lines are usually heterogeneous, comprised of at least two distinct cell phenotypes: neural or neuroblastic N-type an substrate-adherent or Schwann-like S-type It was shortly highlighted that only N-type cells undergo differentiation under RA treatment, while the S-type minority continue to divide [3]. All-*trans*-retinoic acid (RA) is a naturally occurring and biologically active derivative of vitamin A. It is highly sensitive to light, and also to heat and air in solution [8]. The compound is reasonably stable in organic solvents, like DMSO, when it is stored in dark, but in aqueous solution it deteriorates comparably quicker [9].

RA is known to possess powerful properties to arrest the cellular cycle and promote (as well as restore) cellular differentiation. The best characterized neuronal expression marker to quantify RA induced differentiation is β-tubulin. β-tubulin is a cytoskeletal element and is almost exclusively present in mature neurons. Thus, its protein expression level is a well characterize marker and correlates with the earliest phases of neuronal differentiation.

However, there are numerous survival and differentiation activities that are triggered by RA. It has been shown, that RA downregulates the mRNA and protein levels of the differentiation inhibiting basic helix-loop-helix (Id) transcription factors [10]. RA also activates one of the most potent pro-survival signalling cascades, the phosphatidylinositol 3-kinase/Akt signalling pathway in neuroblastoma [11]. Furthermore, via altering survival signalling pathways, the susceptibility to neurotoxins is reduced [12]. It was shown that differentiation affects the resilience of neuroblastoma cells towards energetic stress in the mitochondria via reduced expression of energetic stress response genes. Mitochondria dysfunction and energy metabolism is supposedly involved in neurodegenerative diseases [4].

After treatment with RA, *SH-SY5Y* cells obtain more neuron-like morphological properties as well.

Typically, *SH-SY5Y* cells are exposed to RA at a concentration of 10 or100 µM for a minimum of 3–7 days in serum-free or low serum medium to achieve homogeneous population of cells with neural morphology via inducing their differentiation [1, 12, 13].

To emphasize their effectiveness, it is interesting to mention that a synthetic derivative of all-*trans*-retinoic acid, cis-13 retinoic acid (isotretinoin) is already in clinical use. It showed survival advantages to high-risk bone marrow transplanted patients and a decrease of relapse to patient after therapy and dramatic improvement in case of patient treated with immunotherapy supplemented with isotretinoin [14].

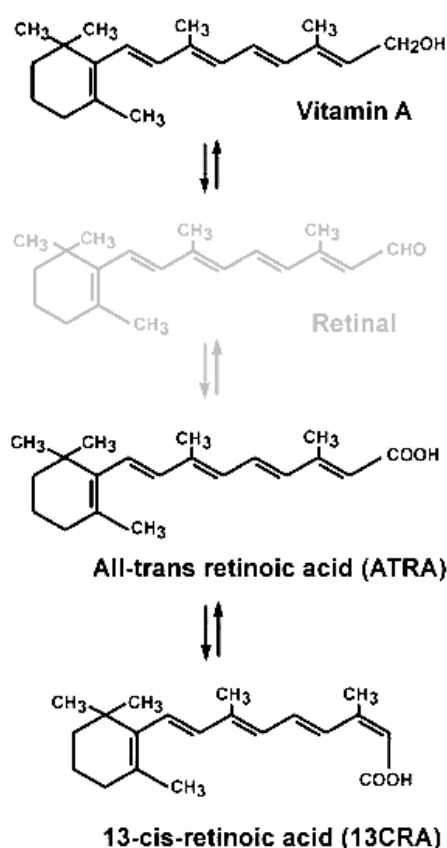**Figure 1.1.1**: All-*trans*-retinoic acid and 13-cis-retinoic acid are derivatives of Vitamin A [15].

1.2. Astrocytes

The second highlighted group of cell present in the brain are the glia cells, non-neural supportive elements. Attention will be drawn to the most abundant population of specialized glia cells, the astrocytes. Depending on the brain region, researcher suggested 1.4-5-10 fold

higher number of astrocytes compared to neurons present [16-18]. The role of glial cells, such as astrocytes in the central nervous system has been difficult to study because glial cells are generally present in CNS cultures and are often essential for neuronal viability.

Astrocytes play a critical role in brain energy metabolism via their direct interaction with the vasculature and direct or indirect connection to the neuron cells. They supply neurons with energy substrates, such as glucose and lactate on demand which in itself could bear some important consequences for our understanding of neurodegenerative diseases [19].

Besides their long associated function of nurturing the neural cells, they are highly targeted in research to understand the neural communication, function and disorder [19].

It has been shown, that astrocytes detect the level of neural activity and strongly regulate neuronal excitability, thus control synaptic transmission and influence neural functions [20]. Other essential, complex functions such as K^+ buffering, and neurotransmitter recycling are also associated with astrocytes [21].

Furthermore, presence of astrocytes displays a critical role for proper neural and development and synaptic connectivity of the healthy central nervous system [20].

Increasing evidence points towards the abnormal consequences of lost function or interaction between astrocytes and neurons. A few researchers have already considered replacing damaged or missing astrocytes to provide support or treatment to the damaged brain. Lepore *et al.* focused at the astrocyte dysfunction in case of ALS. By transplanting astrocyte precursors in specific segment of the cervical spinal cord, they described a promising therapeutic strategy for the neurodegeneration [18].

Besides undeniable importance of cell-cell connections in neurophysiology, the human brain developed through an elaborate series of cellular events, which, following a disruption, can lead to numerous neuropsychiatric and disease. Williams *et al.* suggested a relationship between mental disorders schizophrenia and astrocyte cell density in a specific cortex region [22].

Thus, targeting astrocytes represent an attractive alternative approach to develop new therapies to treat neurological disorders in humans.
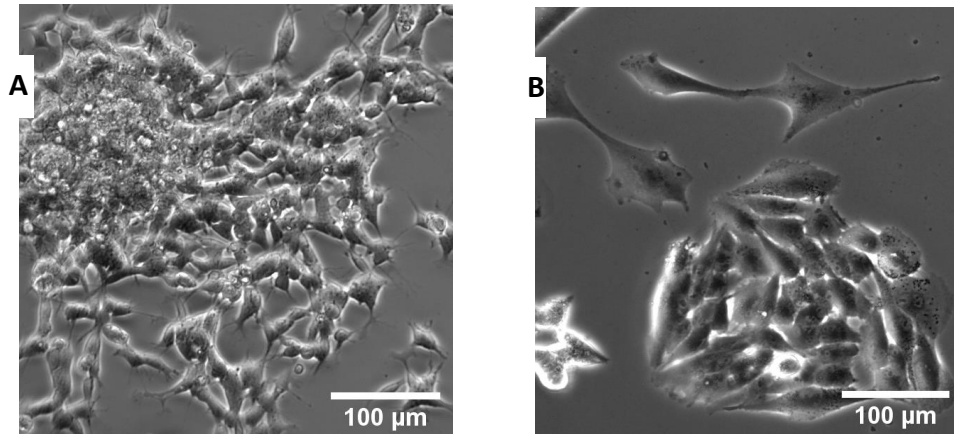
Figure 1.2.1: Phase contrast images of untreated neuroblastoma and astrocyte cells. A) Untreated neuroblastoma island (*SH-SY5Y*) after 7 days of incubation. B) Untreated astrocytes (*HS 683*) after 7 days of incubation. Figure legends alsways under figrue

1.3.   Intercellular connection: role of NrCAM and axonin-1

To establish essential interactions between neurons and glial cells intercellular adhesion is taking place between the cell membranes. One of the mediators for this process is the TAG-1 /axonin-1 on the neural cell model and the NrCAM/Bravo, presented by the astrocytes. The exact binding site of NrCAM on the axonin-1 is still unidentified [23]. However research indicates that the NrCAM's and the associated receptor molecule NgCAM's binding sites on axonin-1 are distinct, but are either close to each other or overlapping. Furthermore, axonin-1 receptors prefers the NrCAM to the NgCAM ones [23]. Both surface molecules belong to the Ig/FnIII subgroup of the immunoglobulin (Ig) superfamily of cell adhesion molecules (CAMs).

Axonin-1 (**Figure 1.3.1**) is an axonal surface glycoprotein expressed on commissural axons [24, 25] . The molecule was shown to mediate guidance signal [23] and by now it is also clear that adhesion molecules generate signals that are crucial in regulating axon growth [26]. Axonin-1 is anchored to the plasma membrane via glycosylphosphatidylinositol (GPI) and contains six Ig-like domains of the C2 subcategory and four fibronectin type III (FNIII)-related modules [27]. Axonin-1's glycolipid anchor may be a signalling route to membrane associated cytoplasmic proteins, such as fyn [28].

NrCAM (**Figure 1.3.1**) belongs to the L1 subfamily of the Ig-CAMs, and is implicated as a specific ligand for another CAM, axonin-1 [28]. NrCAM consist of six extracellular Ig-like domains followed by five fibronectin type III repeats (FnIII), a single-pass transmembrane

region, and a cytoplasmic tail that can bind to and activate cytoskeletal proteins, such as ankyrin [26, 28, 29]. Suter *et al.* identified that NrCAM is predominantly presented by (peripheral) glial cells, but not by neural cells [30]. NrCAM was reported to function as receptor besides serving as a ligand [29]. Knockout studies have indicated that loss or decrease of expression of this protein can lead to changes in cerebellum morphology, eye development and development of the node of Ranvier. It has also been linked to an increased vulnerability to addiction and autism [31].

Li-ning Su *et al.* associated an important role of neural differentiation and development to NrCAM [32]. Sakurai *et al* described, that a certain layer of cerebellar granule cells are NrCAM and TAG-1 positive, and are responsive to a Shh proliferation signal. Upon signalling, they turn F3 positive, and becoming unresponsive to the Shh signal, thus these cells differentiate, and extend the molecular layer forming process [29].

Members of the L1 family are stimulating neurite growth [23]. Growing axons find their destination by integrating positive and negative guidance cues along their trajectory. The guidance cues are molecules secreted from intermediate or final targets, or are displayed in the extracellular matrix or on the surface of cells along the axons' pathway [23]. An interaction between neuronal axonin-1 and NrCAM is suggested to play a crucial role in the axon guidance across the midline of the spinal cord in the peripheral nervous system (PNS) [23][26][25][30] furthermore in the function regulation of the central nervous system (CNS) [31, 33].

It is believed that one single membrane-spanning protein cannot generate intracellular signals in response to extracellular events without associating with another transmembrane protein [26]. Upon cellular activity change due to the interaction with either RA or NrCAM or both, it is assumed that neuroblastoma cells start a differentiation process. This process can be quantitatively evaluated by following ß-tubulin expression values.

Another, axonin-1 associated protein, fyn-kinase is an important indicator in cancerous cells, such as neuroblastoma, since it was shown to contribute to the development and progression of several cancer types via controlling cellular growth, death, morphogenic changes and motility. Enhanced expression and/or activation of Fyn is associated with the malignancies of brain cancer[34].

A decreases in fyn expression in the axonin-1 hosting neuronal cells upon cellular interaction between axonin-1 and NgCAM, which shows an active intracellular signalling cascade [35].
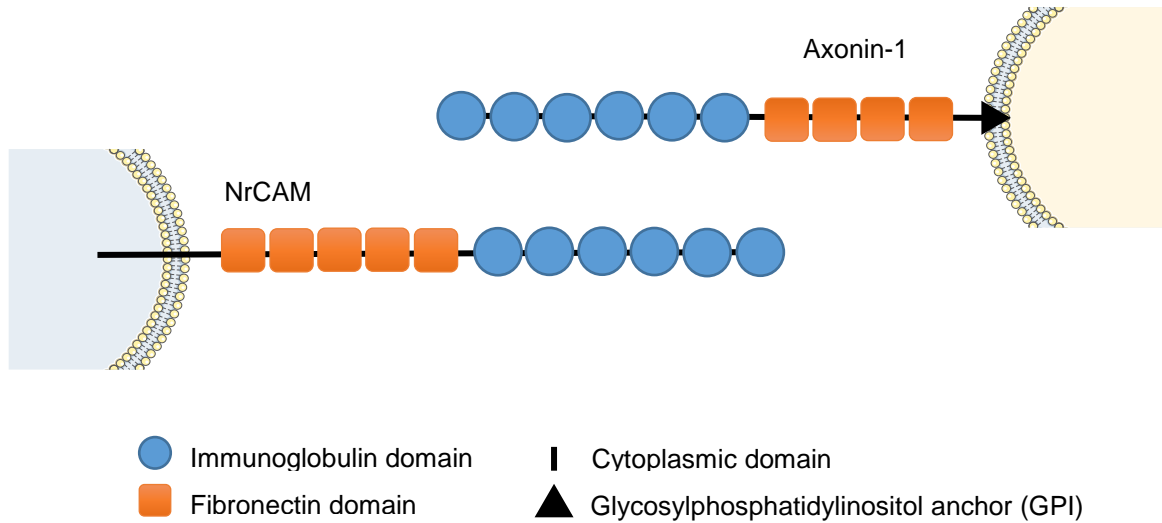
Figure 1.3.1: Schematic representation of NrCAM and Axonin-1 bound to astrocyte and neural cell membrane, respectively

1.4.   Nano- and micrometer-sized lipid vesicles

Compartments are the fundament for cellular life, providing chemical and physical barrier from the surroundings as well as spatially and temporally controlled environment for metabolic and transport functions, synthesizing processes and signalling activities [36-38]. To understand the complexity of cellular dynamics, simplified models of cells and membrane based cellular compartments have been developed and studied using principles of synthetic biology [36, 38], scientists could endow artificial cells with cellular functions inspired by natural systems.

Necessary to mention, that there are some differences between natural and synthetic extracellular vesicles, however, due to the development of latter, many fundamental characteristics of the natural counterpart can be mimicked taken advantage of the minimal, controllable, modular synthetic systems [39]. Another important factor is their size, which can vary between 20 nm- 1 μm [40].

1.4.1. Synthetic cells

The synthetic biology approach to mimic biological compartments is via bottom-up assembly of protocell model systems. In this context, protocells are basically liposomes;

synthetic, lipid-based compartments with an aqueous volume entrapped by one or more bilayers created under physiological conditions.

One of the most common method is to create lipid-based giant unilamellar vesicles (GUVs) (**Figure 1.4.1 B**) from supported phospholipid bilayers, which can provide a close resemblance to natural cell membranes [41]. It is a very important tool to investigate and decipher specific behaviour upon mixing model and real biological membranes, as well as to functionality and dynamics of bio membranes, furthermore to mimic single biological events in a synthetic environment.

Vesicles can also be formed using amphiphilic block copolymers. Copolymer-stabilized water-in-oil compartments, crafted using microfluidics, can be precisely controlled and produced in an automatized manner [36]. Moreover, depending on the environment, self-assembling behaviour can be observed based on the molecular structure in order to minimize the selective block-block interactions with the solvent which is energetically unfavourable for the system [42].

Using this well-defined copolymer-stabilized water-in-oil droplet micro-environment, and determined concentration of phospholipid in the physiological aqueous phase, GUVs can be fabricated inside the copolymer shell or copolymer droplet [36][38]. This process results in the so-called droplet-stabilized giant unilamellar vesicles or dsGUVs, shown in **Figure 1.4.1 A**.

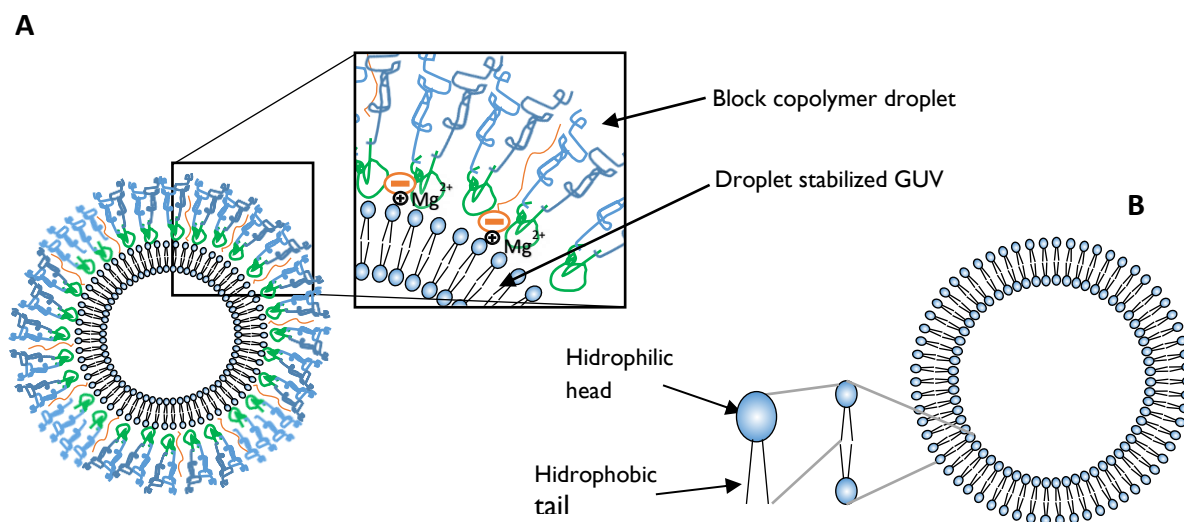**Figure 1.4.1:** Charge controlled formation of dsGUVs. A) Sketch of a GUV encapsulated into a water-in-oil droplet stabilized by inert PFPE-PEG based surfactant containing PFPE- carboxylic acid with negatively charge. The droplet formation is mediated by 10 mM Mg^{2+} and the charged lipid constituent. B) Schematic representation of a giant unilamellar vesicle after release, showing the hydrophilic and hydrophobic regions.

In this project, a shear stress emulsificator was used to create dsGUVs as described in section 2.2.2.2 GUV creation and release SUV production in chapter 2: Materials and methods. Using this method, the production is very quick and easy compared to the microfluidics or electroformation approach, since it is sufficient to test our hypotheses [38, 43].

This system requires a necessary amount of charged surfactant molecule in the polymer shell, which will eventually start the charge-driven alignment of the phospholipid assemblies at the periphery. As an example, if the hydrophobic head group of the chosen polymer is chemically inert, as uncharged PEG, then it creates repulsive interaction between the droplet shell and the different lipid-assemblies. By adding a negatively charged fluorosurfactant, for example, PFPE-carboxylic acid, it will competitively assemble on the internal periphery of the droplet [38].

The confined aqueous solution for GUV production is made from the determined lipid composition, physiological buffer (e.g. PBS), and $MgCl_2$ [38]. The aqueous solution in the buffer already contains self-assembled structures, e.g. micelles or multilamellar vesicles due to the amphiphilic characteristics of the lipids.Mg^{2+} is needed to form the lipid bilayer in case the polymer shell presents a slightly negative charge. The negatively charged regions of the internal droplet interface first attract the Mg^{2+} ions from the lipid-buffer solution. As follows, the lipid molecules rupture from their assembled form and start to interact to the Mg^{2+} ions, which results in a supported lipid bilayer at the droplet periphery.

Haller et al. [38] showed a necessity of 6-13.5mM range of the charged fluorosurfactant in a 1.4 % PEG-based surfactant solution for efficient GUV formation. Furthermore, the lipid composition is required contain at least 10 % negatively charged lipids to the optimal production.

The created lipid vesicles can be released from the stabilizing polymer shell (surfactant oil phase) to a physiological environment, which allows us to functionalize the GUVs or to present them to cells or extracellular matrices [36]. An easy way to release the GUVs is by bulk release. This is performed by addition of a demulsifier/emulsion breaker surfactant (here 1H,1H,2H,2H-Perfluoro-1-octanol) and the used buffer without $MgCl_2$. This way the perfluorooctanol replaces the fluorinated oil surfactants from the water-oil interface, increasing the intermolecular distance and weakens the binding forces constructed by the emulsifier (consequently lowering the free energy of the system) so that the aqueous phase can separate from the oil phase.

1.4.2. Importance of spheroids

The culture of cells on two-dimensional (2D) surfaces has provided groundbreaking insights into basic cell biology and tumorigenesis [44]. However, this condition does not faithfully mirror the *in vivo* situation because most physiologic parameters of tumors or organs such as proper tissue architecture and complex cell-cell or cell-matrix contacts, mechanical

properties as well as biochemical networks are not applicable in such 2D systems [45, 46]. Monolayer studies are also limited in imaging and high-throughput studies [46].

Traditional animal studies provided the foundation for understanding organ functions and now highlighting brain functions and development, however, these studies were limited by the shared properties between vertebrates and human brain [47]. Furthermore, new bridge models are increasingly demanded due to ethical considerations between in vitro and in vivo experiments. Recently for this purpose, organoids are created. Organoids are stem cell derived near native tissue structures as in morphologically and architecturally comparable as well as functionally similar to the given organ that is created by recapitulating development and self-organization [48]. Organoids can be used for example for organ repair dissociating stem cells into one or more mature cells and re-create the organ in vitro [49] or can be considered as one tool paving the way towards personalized medicine [47].

As 3D culture, spheroids (**Figure 1.4.2**) can represent the transition model between 2D models and organoids. In fact they can be generated and grown from stem cells all the way to organoids [50].
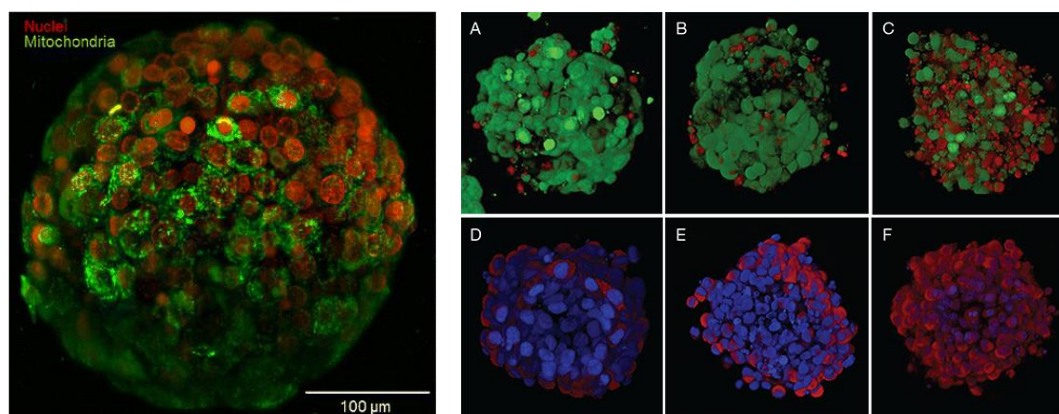
Figure 1.4.2: Left: T-47D tumor spheroids imaged by light-sheet-based fluorescence microscopy (LSFM) [51]. Right: Viability and oxidative stress assessment with HeLa spheroids, picture adapted by Thermo Fisher:

Three dimensional (3D) cell cultures are well documented to resemble intrinsic properties of a specific organ or tumour and better mimic the *in vivo* circumstances compared to cells cultured as 2D cell growth on plastic surface [45]. Furthermore, they are less complex, less cumbersome non-exclusively stem cell derived models compare to organoids to study behavior, bioavailability, and drug responses on specific tissues. They provide a unique opportunity to recapitulate aspects of cell homeostasis and intercellular adhesion and eventually events to dictate cellular fate [52]. Studies have shown that the gene expression characteristics [53] as well as the responses to treatment [54] in the multicellular spheroid 3D models resemble more closely the in vivo situation than monolayer counterpart. Riedl et al demonstrated significant differences of PI3K/Akt/mTOR signaling (Pi3k/Akt is a very

important pathway in the context of RA mediated differentiation) in the 3D vs the 2D system, including spatial alterations in the signaling intensity and responses to inhibitor treatment [46].

Three dimensional culture generally estimates the drug efficiency better because of the presence of physico-biochemical barriers [55]. Therefore, 3D cancer models are increasingly acknowledged and biologically relevant for bioavailability testing, drug development and preclinical drug testing [46].

By introducing different cell types in the 3D culture, creating a co-culture, it would lead to the formation and possibly the spatial self-organization of diverse tissues within a single organoid [49]. Co-cultures are fundamental to study cell–cell interactions occuring at different length/time scales, which is important for example to infection studies, drug targeting, population control, complex cell behaviour and drug research [56]. As to neuronal-astrocyte co-culture, survival and function of neurons are remarkably dependent on glial cell support, and even in vitro glial cells were shown to control the number of synapses and increase the synaptic efficacy in neuronal cultures. Direct proximity of neurons to glial cells has been shown to be crucial to their interfacial interactions and long-term potentiation, a mechanism that (in vivo) underlies learning and memory [57]. Thus, to ensure that cultured neurons resemble their vivo situation more accurately, it is important that they are cultured close together with glial cells [58].

1.4.3. Spheroid generation

There are different methods to generate 3D cultures, such as 3D collagen gel [45] bioreactors, hanging drops or via microfluidics [59], or one of the newest procedure, inside naked liquid marbles [60]. Many of these protocols are complex manual work causing cellular and metabolic stress. The aim of microfluidics is to create an easy, high throughput system that can also provide *in vivo*-like surrounding. This can be achieved by controlling the droplet generation by adjusting the flow rate, the temperature and the constitution of the medium. With droplet-based microfluidics, cells are flowed through micro tubing system where they are exposed to a flow of oil surfactant, which cuts of droplets filled with the cells and media.

Using microfluidics, highly monodisperse droplets can be generated at rates greater than 1000 droplets/min, furthermore live imaging and downstream analysis can be integrated [61]. Most of the times, a scaffold, agarose, gelatine, alginate, PEG as well as mixed hydrogels such as alginate-Matrigel is used as scaffold to direct the spheroid formation [61]. To overcome some of the mentioned limitations, we exerted a scaffold free (only culturing media) droplet based microfluidic system allowing mass fabrication of 3D co-culture spheroid models. This way the direct proximity of neuronal and glial as well as neuronal and synthetic vesicles can be provided, furthermore supported by technical controllability and stability [58]. The

depletion of the nutrients inside the micro sized droplets was estimated by around 24 hours after incubation, thus the spheroids were recovered by disrupting the surfactant-oil droplets using perfluoro-octanol and grown in media for 7 days [55].

1.5.   Microfluidics

Microfluidic devices can be used for high-throughput production of monodisperse copolymer-stabilized water-in oil compartments (droplets), as well as the aforementioned dsGUVs.

We used droplet based microfluidics which provides a controlled production and a confined volume, consequently close proximity to the cells for their interactions.
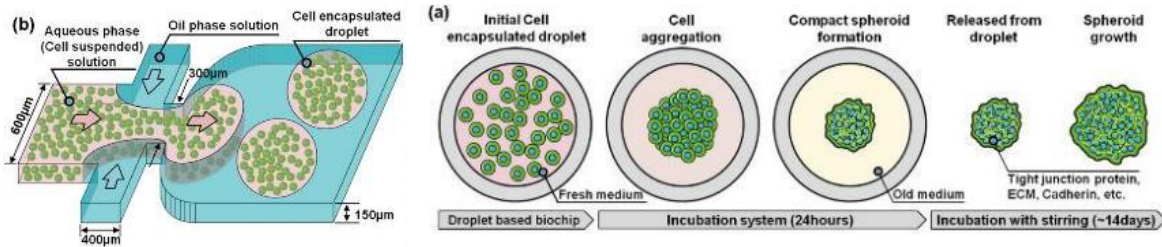
Figure 1.5.1: Droplet based spheroid generation adopted by Kwak *et al.* [55]

The microfluidic devices are made of PDMS on a silica wafer containing a design made by photolithography [62][63]. The devices were assembled with plasma treatment where on exposure to oxygen plasma, silanol groups (Si-OH) are formed on both material. In close contact with glass surface, the reaction yields Si–O–Si covalent bonds after loss of a water molecule. Thus, after the treatment, the devices were mounted together immediately, so that the reduction of the created reactive residues are minimized [64]. For producing water-in-oil droplets, surface modification was necessary. The used Ombrello mix (highly acidic) creates a hydrophobic surface, thus the aqueous phase is unable to react with the surface of the small tunnels of the device. High uniform droplets are created at the flow-focusing T-junction of the perpendicular streams, where the aqueous phase is encountering the surfactant oil phase. Using pressure-pumps, and applying a well controllable flow rate, stable droplet production can be achieved with a rate of around 1 kHz [41].

1.5.1. Surfactants and buffers

For droplet production *via* microfluidics, shaking or the shear stress emulsifying, one key parameter is the stabilizer surfactant used.

To generate GUVs, stability and charge on the periphery of the droplet was indispensable, and for this purpose, fluorinated oil, FC-40 was mixed with 1.25mM fluorinated surfactant. We use an in house synthesized triblock-copolymer surfactant is composed as followings: Perfluorpolypropylene–Polyethylene glycol-Perfluorpolypropylene (PFPE-PEG-PFPE) (**Figure 1.5.2 B**).

The perfluorinated polyethers (PFPE) carboxylic acid surfactant with hydrophobic tails provided the negatively charge and measurable stability to the droplets by preventing coalescence. The hydrophilic head group block of the amphiphilic fluorosurfactant molecule is composed of the poly(ethylene glycol) (PEG) moieties, which serves as a biocompatible, inert interior surface of the aqueous drops [41].

In case of cell encapsulation, the stability and the prevention of charges on the droplet inner layer was important to consider. Charges were concluded to negatively influence the spheroid formation since cells themselves being slightly charged are electrostatically drawn to charged particles or surfaces [65][66]. For this purpose, commercially available non-charged fluorosurfactant can be combined with non-charged fluorinated oil HFE7500 (**Figure 1.5.2 A**) in a total 5(w/v)% concentration.

At the critical micelle concentration, water-in-oil droplets are assembling thus confining the aqueous phase more precisely pH 7.4 PBS buffer (Phosphate Saline Buffer) which closely mimics the pH, osmolarity, and ion concentrations of the human body [67][68].
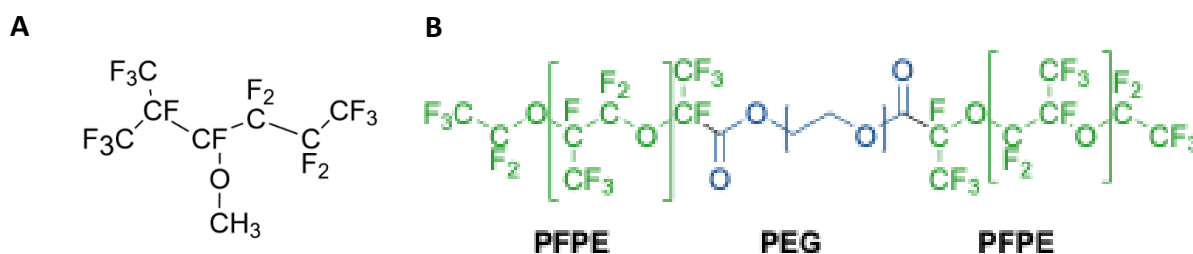

Figure 1.5.2: **A:Hydrofluoroether (HFE) B:**Perfluorpolypropylene–Polyethylene glycol-Perfluorpolypropylene (PFPE-PEG-PFPE) molecule

1.6. Project aims and scope

The aim of this project is to generate co-cultured spheroids of neuroblastoma and astrocyte, as well as creating semi-synthetic co-cultured spheroids with a droplet based microfluidics platform. The semi-synthetic spheroid is assembled by introducing a minimal synthetic astrocyte architecture into the neuroblastoma spheroid. Towards this end, droplet stabilized GUVs are created *via* shear stress emulsification. These GUVs are biofunctionalized *via* His -tag chemistry with NrCAM cell adhesion molecules, thereby mimicking a pivotal astrocyte functionality. An interaction between the neuroblastoma cells and the GUVs is hypothesized to act according to naturally occurring interactions between the NrCAM ligand on astrocytes and the axonin-1 cell adhesion molecule, latter presented by the neuroblastoma cells. To characterize the created co-cultured and semi-synthetic spheroids, differentiation and associated cellular morphology in 2D and 3D cultures are evaluated. To assess differentiation tendencies, a western blot quantification method will be established, focusing on the well characterized neural expression marker, β-tubulin. Eventually, integration of synthetic astrocytes into neuronal spheroids, by means of droplet based microfluidics, will not only allow for high precision assembly of spheroids with increased homogeneity, but also to decipher individual, NrCAM associated processes involved in neuroblastoma differentiation.

Chapter 2

2.Materials and methods

2.1.   Materials

Table 2.1.1: Table of chemicals

Name	Description	Supplier
DOWSIL - SYLGARD™ 184 Silicone Elastomer	GMID - 01673921	The Dow Chemical Company
SYLGARD™ 184 Silicone Elastomer Curing Agent	GMID - 01673921	The Dow Chemical Company
Extran MA-01	1.07555.2500	Merck
Ombrello TM	13356003N	moton automotive
Flouriniert FC-40	CAS Number 86508-42-1	Merck/Sigma-Aldrich
JW100 10mM in FC-40	PFPE7000-PEG600-PFPE7000	In house
JW106 10mM in FC-40	PFPE2500-PEG600-PFPE2500	In house
FluoroSurfactant	Lot#031-017	RAN Biotechnologies
HFE7500/Novec7500	FL-0004-HP-1000	IOLITEC
DPBS 1x	REF:14190-144	Thermo Fisher Scientific
1H,1H,2H,2H-Perflouro-1-octanol	Lot:MKCG4799	Sigma-Aldrich
Magnesium chloride	M2670	SigmaAldrich
NuPAGE™ MOPS SDS (20X)	NP0001	Thermo Fisher Scientific
NuPAGE™ Transfer Buffer (20X)	NP00061	Thermo Fisher Scientific
SurfactAway™ Non-ionic Triton Removal	SA890-30	Biotech Support Group

Table 2.1.2: Table of biologicals used in the experiments

Name	Description	Supplier
DMEM, high glucose, GlutaMAX™ Supplement, pyruvate	31966047	Thermo Fisher Scientific
DMEM/Ham's Nutrient Mixture F12	51448C	Sigma Aldrich
Penicillin-Streptomycin (10,000 U/mL)	15140122	Thermo Fisher Scientific

Fetal Bovine Serum (FBS)	F7524	Sigma Aldrich
Albumin Fraction V (BSA)	8076.3	Carl Roth GmbH
Trypsin-EDTA (0.05%), ph. red	25300062	Thermo Fisher Scientific
Egg PC	840051	Avanti polar lipids
Egg PG	841138	Avanti polar lipids
Liss Rhod PE	810146	Avanti polar lipids
DOBAQ	850310	Avanti polar lipids
CellTracker blue CMAC	C2110	Thermo Fisher Scientific
CellTracker Green CMFDA	C7025	Thermo Fisher Scientific
HOECHST 33342	H3570	Thermo Fisher Scientific
WGA-Alexa647	W32466	Thermo Fisher Scientific
NrCAM	8425-NR-050	R&D Systems
IgG-Alexa647	#A31571	Thermo Fisher Scientific
Anti-E-cadherin	#610181	BD Biosciences
Novex Sharp Pre-Stained Protein st.	LC5800	Thermo Fisher Scientific

Table 2.1.3: Table of cells used for the measurements

Cell name	Description	Cell type	Source	Provider
HaCat	#330493	Endothelial	Homo sapiens	Cell Line Service
HS-683	HTB138	Astrocyte	Homo sapiens	ATCC
SH-SY5Y	#300154	Neuroblast	Homo sapiens	Cell Line Service

Table 2.1.4: Table of materials used in the experiments

Name	Description	Supplier
Harris Uni-Core punch 0.75mm	US Pat.no.7093508	Sigma-Aldrich
Extruder	Avanti#610023	Avanti polar lipids
HAMILTON 1000 uL syringe	Avanti# 610017	Avanti polar lipids
Whatman Nucleopore Track-Etch membrane 0,05µM 19mm	13113512E	Sigma-Aldrich
Support filter 10mmx100µm	Avanti#610014	Avanti polar lipids
Sarstedt Inc T75 Culturing Flask	Cat no. 50-809-261	Thermo Fisher Scientific
CELLSTAR® 6-well plate	Art.-Nr.: 657160	Greiner Bio-One International
Brown vial	L/N:6114580860	SUPELCO
picodent twinsil® 22	1300 1000	picodent
Nitrocellulose Membrane, 0.45 µm, 30 cm x 3.5 m	88018	Thermo Fisher Scientific
Bolt™ 4-12% Bis-Tris Plus Gels, 12-well	NW04122BOX	Thermo Fisher Scientific
Blotting Filter Papers, 2.5 mm thickness, 7.5 cm x 8.4 cm	LC2010	Thermo Fisher Scientific

2.2. Methods

2.2.1. Device production

Microfluidic devices were produced as previously described [69][70]. Device wavers were either produced in house by the described photolithography technique or produced in house by milling the designed channel structures into PMMA via milling by CNC machine. For the device assembly, both the glass slides and the PDMS (The Dow Chemical Company) chip was exposed to oxygen plasma treatment (TePla, TePla-100e) for 35 seconds on 200W and 0.4 mbar.

2.2.1.1. Droplet production

Water-in-oil droplets were produced with the microfluidic device via flow focusing at the T-junction of the device using differently adjusted flow rates. Flow rates were controlled by Elveflow OB1 MK3 pressure system (ELVESYS), which allowed pressure setting around 110 mbar for the water phase and 130 mbar for the oil phase to create stable droplets. For the cell suspension, the cells were trypsinized (Thermo Fisher Scientific), counted and the targeted cell concentration was prepared in respective cell culturing media.

For microfluidic encapsulation of neuroblastoma (*SH-SY5Y*, ATCC) as well as neuroblastoma-astrocyte (astrocytes: *HS 683*, Cell Line Service) co-cultured cells with microfluidics, in order to test the immunofluorescent staining, 2,5mM JW100 surfactant in FC-40 was used as oil phase. For the western blot samples, an oil emulsion was produced using non-ionic 5% FluroSurfactant (RAN Biotechnologies) in HFE-7500 (Novec7500 IOLITEC) and the cell suspension with a cell concentration of 10 to 20 million cell/ml was introduced to the aqueous inlet.   The cell culturing media in this instance was F12 media (Sigma Aldrich), with 1% Penicillin/Streptomycin (Thermo Fisher Scientific) and 1% FBS (Sigma Aldrich).

2.2.2. GUV production

2.2.2.1. Lipids

To create the synthetic minimal astrocyte, and the minimal GUVs (for the standard curve) the following lipids were used : L-*a*-phosphatidylcholine (from chicken egg - EggPC), L-*a*-

phosphatidylglycerol (from chicken egg - EggPG), 1,2- dioleoyl-sn-glycero-3-phosphoethanolamine-N-(lissamine rhodamine B sulfonyl - LissRhod), 1,2-dioleoyl-sn-glycero-3-[(N-(5-amino-1-carboxypentyl)iminodiacetic acid)succinyl] (nickel salt) (18:1 DGS-NTA(Ni)) (Avanti polar lipids).

EggPC (**Figure 2.2.1, A**) contributed as main non-charged lipid component, EggPG (**Figure 2.1, B**) was used to achieve a negative charge on the GUV periphery which contributed to the charge-driven vesicle formation.

LissRhod (**Figure 2.2.1, C**) as a rhodamine B labeled lipid was used for detection due to its fluorescent excitability. Rhodamine B is a fluorescent dye to the conjugated p system in its aromatic rings, which can be excited at 550 nm wavelength and detected in 560-620 nm range with fluorescence microscopy [36]. The emitted light was measured during plate reader experiments and allowed the GUV imaging with confocal microscopy and.

DGS-NTA(Ni) (**Figure 2.2.1, D**) is an NTA tagged lipid with a nickel(II) atom incorporated. This component was used to conjugate NrCAM (R&D Systems) with its C-terminally syntehsized His-tag to the GUVs by NTA-Ni^{2+}. The recombinant NrCAM purchased contains the Leu30-Pro 630 region of the human NrCAM protein.
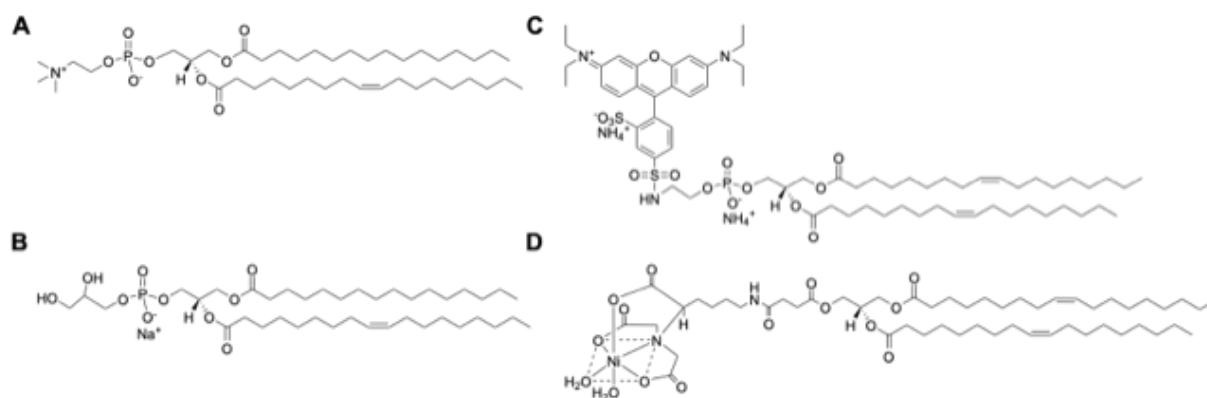

Figure 2.2.1: A: EggPG; B: EggPC; C:LissRhod; D: DGS-NTA adopted from Avanti polar lipids.

2.2.2.2. SUV production

Table 2.2.1 and **Table 2.2.2** shows components and composition of SUV and GUV mixtures used for production of NrCAM functionalized GUVs and associated standard curves.

Standard curves were prepared by serial dilution of the SUV mixture (3000µM, 2000µM, 1000µM, 500µM, 250µM, 125µM, 62.5µM, 31.25µM, 15.625µM, 7.8125µM) and respective fluorescence intensity was measured with a TECAN plate-reader using excitation

wavelength 550 nm and emission wavelength 585 nm using automatic gain optimization settings. Linear regression fitting was used to determine a concentration standard curve from which GUV concentration after cleaning was deduced.

Table 2.2.1: Basic GUV composite for creating concentration standard curve, 6000µM

Lipid	M [g/mol]	c [mg/ml]	c [mM]	ratio	c final [uM]	V final [uL]
Egg PC	770,1	25	32.5	79	4121,7	38,09
Egg PG	782,3	25	32	20	1565,2	14,69
Liss Rhod PE	1301,7	1	0.8	1	52,2	20,37

Table 2.2.2: NTA containing GUV-s, 6000 µM

Lipid	M [g/mol]	c [mg/ml]	c [mM]	ratio	c final [uM]	V final [uL]
Egg PC	770,1	25	32,5	78	4680	43,25
Egg PG	782,3	25	32,0	20	1200,0	11,26
Liss Rhod PE	1301,7	1	0,8	1	60,0	23,43
DGS-NTA(Ni)	1057,0	10	9,5	1	60,0	1,90

The required amounts of the lipid composites were pipetted into a 1 mL glass vial and the lipid solvent chloroform was evaporated using a gentle nitrogen stream. The lipid layer was re-hydrated with PBS (gibco/Thermo Fisher Scientific) buffer with 10mM MgCl$_2$. After 5 minutes hydration, the lipids were vortexed gently for 2 minutes to create a mixture of polydisperse multilamellar vesicles. For extrudering the SUVs, mechanical extruder (Avanti Polar Lipids, Inc.) was assembled with a 50 nm pore radius polycarbonate membrane filter (Avanti Polar Lipids, Inc.). The resulting SUV dispersion was extruded carefully 9-11 times using the extruder from Avanti and diluted to 3000µM in additional PBS with 10 mM MgCl$_2$.

2.2.2.3. GUV creation and release, SUV production

For GUV production, oil surfactant phase was prepared with fluorinated FC-40with in-house synthesized triblock copolymer surfactants, JW104 (PFPE7000-PEG750) and JW106 (PFPE2500-PEG600-PFPE2500) diluted in a final concentration of 1,25mM. GUVs for the standard curve were produced using JW104, while for the biofuncitonalized GUVs, JW106 surfactant was chosen. The method of surfactant synthesis was previously described by Platzmann *et. al* [41]. The mix of the aqueous SUV-phase and the surfactant oil phase was 1:4. The PBS buffer for GUV production was supplemented with 10mM MgCl$_2$. Droplet stabilized GUVs (dsGUVs) were created through mixing the emulsion of the aqueous SUV phase and the surfactant oil phase with high shear stress emulsificator on

level 5 for 1 minute (IKA T10 basic ULTRA-TURRAX disperser). The mixture was set incubate at 4°C for 1h for complete phase separation. Subsequently, the highest possible volume of the excess oil phase was discarded by pipetting to remove excess surfactant.

For the release, Mg^{+2} free PBS buffer and destabilizing surfactant (1H,1H,2H,2H-Perflouro-1-octanol, Sigma-Aldrich) were added to the droplets in equivalent volume to the created SUV aqueous phase volumen. If needed, some additional destabilizing surfactant and buffer were added to improve release efficiency and demulsification. Afterwards, the tube was gently rotated to support the release by gentle mixing. The top aqueous layer contained the created GUVs, which for biofunctionalization, were further cleaned from rupture SUVs or excess lipids by cleaning as described in the next chapter.

2.2.2.4. NrCAM functionalized NTA-containing GUV-s

The gained GUV solution was cleaned through 5 minutes centrifugation 9486 RCF. The supernatant was discarded and the pellet was resuspended in PBS to the same volume as it was before cleaning.

NrCAM (R&D Systems) was reconstituted to 500µg/mL in sterile PBS. Before incubating the NrCAM with the GUVs, the final mass of the presented NTA-ligand was calculated by evaluating the release efficiency via standard curve measurements (see section 3.3.2 Functional assessment by Western blot analysis). Considering that one NTA is reacting with one NrCAM molecule, the respective volumes of NrCAM can be calculated and mixed with the GUV dispersion 20 minutes before application.

2.2.3. Cell culturing

- Cell culturing medium

Astrocytes (*HS683*, ATCC) and *HaCat* cells (Cell Line Service) were routinely culture on DMEM (gibco/Thermo Fisher Scientific) cell culture medium supplemented with 1 % Penicillin/Streptomycin (Thermo Fisher Scientific) and 10 % fetal bovine serum (FBS, Sigma Aldrich) at 37°C, 5% CO_2 atmosphere and 100% humidity.

For culturing the neuroblastoma cells (*SH-SY5Y*, ATCC), F12 medium (Sigma Aldrich) with 1 % Penicillin/Streptomycin and 10 % of FBS was prepared. During experiments, to induce differentiation, the medium was supplemented with only 1% FBS. Cells were passaged at ~90% confluency based on 0.05% trypsin/ EDTA (Thermo Fischer Scientific) treatment.

2.2.3.1.   Cell plating

Cells were counted after trypsinization using Neubauer chamber. For the morphology assays and for the western blot samples, varying cell concentrations of astrocytes and neuroblastoma cells were seeded into non-adherent flasks (Thermo Fisher Scientific) for 3D cultures and into 6-well plates (Greiner bio-one International) for 2D cultures. To conditional comparability, both in case of 2D and 3D samples for western blotting, the cells were resuspended in 2 ml cell culturing media in the respective culturing product. In case of the *HaCat* experiments, the volume varied depending on the targeted cell concentration. Regarding the neuroblastoma and the co-culture on 6-well plates, cells were seeded in medium containing 10% FBS, and after 1 day the medium was changed to 1% FBS. Cells in flasks were seeded using 1% FBS directly. Retinoic acid concentration was optimized using the recommended $2.5*10^5$ cell/ml concentration and three optional retinoic acid concentration: 1mM, 100µM and 10µM. After optimization, only the best performing concentration was used.

2.2.3.2.   Cell release, fixing and staining

During preliminary testing *HaCat* cells were encapsulated into droplets and released to pre-test the conditions and the devices. Cells were entrapped into droplets created by manual shaking. The microfluidic encapsulation of *HaCat* cells is described in chapter 2.2.1.1.Droplet production. For the shaking method, 300µL of the oil phase, made of 1.25mM JW100 surfactant in FC-40 was used and 200µL of cell suspensions with different cell concentration (1-1,5-2,5-5 million cell/ml) in culturing media (DMEM, 1% Penicillin/Streptomycin and 10%FBS). The spheroids were released after 24 hours.

To characterize spheroid formation as well as immunofluorescent staining by imaging, neuroblastoma, and neuroblastoma-astrocyte co-culture droplets were produced *via* microfluidics and shaking. The microfluidic approach was described in 2.2.1.1.Droplet production. For the shaking method 300µL FC-40 with 1,25mM JW100 surfactant, and 200µL cell suspension with 1 million cell/ml cell concentration (media: supplemented F12, with 1% Penicillin/Streptomycin and 1%FBS) was used. The spheroids were released after 24 hours.

- Cell release

    For spheroid release, the excess surfactant after phase separation was discarded by withdrawing droplet-free oil. 1,5x volume of the starting aqueous phase of destabilizing surfactant (1H,1H,2H,2H-Perflouro-1-octanol) and PBS were added. After gentle rotation in hand, the phases separated and the spheroids were released.

- Cell staining

For live cell staining, released spheroids were incubated with 50 µl of a staining master-mix per sample composed of: 50µL of PBS, 10µL WGA-Alexa647 (Thermo Fisher Scientific) (1mg/ml) and 0,25 µL HOECHST 33342 (Thermo Fisher Scientific) (2 µg/ mL). Cells with the staining solution were incubated for around 5 minutes, which was followed by 5 minutes centrifugation at 5018 RCF. The spheroid pellet was resuspended and fixed with 4% PFA as described in the next section (Cell fixing).

- Cell fixing

For microscopical analysis and immunofluorescent staining, the created spheroids were chemically fixed. To this end, ~200µL released spheroid solution were added to 400µL PBS. From this, 500µl were transferred to a new Eppendorf. 1mL of 4% PFA was added to the samples making up a PFA concentration of 2,67% and incubated for 10 minutes. The spheroids were centrifuged for 5 min at 5018 RCF. 1400µL of supernatant were discarded. The sample was resuspended in the remaining 100 µL.

- Immunofluorescent staining

Immunofluorescent staining was pre-tested on *HaCat* spheroids. After the previously described PFA treatment the spheroids were spinned down on a the table top centrifuge (5018 RCF, 5 minutes) The supernatant was discarded and the cell pellet was re-suspended in 1mL 0,05% Triton-X (Biotech Support Group) dissolved in PBS. Immediately afterwards, the sample was centrifuged again at 5018 RCF for 5 minutes. Subsequently, the supernatant was discarded again and the sample was resuspended in 1mL of 1% BSA (Carl Roth GmbH) (in PBS), followed by 30minutes of incubation in the dark while gentle agitation on a horizontal shaker. Afterwards, the spheroids were spinned down at 5018 RCF for 5 minutes. Anti-E-cadherin (BD Biosciences) primary antibody was diluted in 1% BSA to the manufacturer's recommendation (1:500). After discarding the supernatant, the sample was re-suspended in the primary antibody solution and incubated while gentle agitation for 1-2 hours on the horizontal shaker in the dark. Subsequently, the spheroids were centrifuged again, the supernatant was discarded and again 400µL 1% BSA was pipetted on the sample. This was then supplemented with the fluorescently labeled secondary anti-mouse IgG-Alexa647

(Invitrogen/Thermo Fisher Scientific) antibody diluted to 1:500 in 1% BSA (Carl Roth GmbH). The samples were then again incubated on the horizontal shaker for 30 minutes in the dark. At last, the sample was spinned down at 5018 RCF for 5 minutes on table top centrifuge, the supernatant was discarded and the sample was re-suspended in 400-1000µL of the 1% BSA solution (depending on the amount of collected spheroids).

- Staining for cell differentiation and imaging

Neuron-astrocyte spheroid formation inside the droplets was followed with CellTracker Green (Thermo Fisher Scientific) and CellTracker blue (Thermo Fisher Scientific) staining . Each dye was applied in 5µM concentration and was incubated with the cells for 30min. After the incubation time, the cells were centrifuged for 5 minutes on 5018 RCF.

2.2.4. Microscopy

- Staining

In order to image the spheroid, WGA-Alexa Fluor647 and HOECHST 33342 dyes were used. WGA-Alexa Fluor647 is a carbohydrate binding lectin which is perfect for membrane staining in deep red range (excited at 647 nm, with emission maxima around ~668 nm). HOECHST 33342 enters the cell nucleus and binds to the DNA, it can be excited between 352-392nm and measured between 440-461 nm wavelengths.

To distinguish between the astrocytes from the neurons, cell tracker dyes was employed which are well retained and non-toxic at working concentration. They can freely pass through cell membranes into cells, where they transform into cell membrane-non-permeable reaction products. CellTracker Green has an excitation maxima around 492 nm and emission peak at ~517 nm. Cell Tracker blue can be excited around 372nm and its emission maxima is ~470 nm wavelength.

2.2.4.1. Confocal microscopy

In this project, laser-scanning confocal microscopy was used to resolve the structures inside droplets and spheroids. Confocal microscopy provides a dramatically better contrast and definition compared to conventional light microscopes. In case of the traditional epi-fluorescence microscopes after illuminating the samples, the emitted light often times occurs through the full volume of the excited sample, which in case of a thicker sample

leads to loss of details.

Confocal microscopes use an intense, coherent, excitation light source, a laser. The field of illumination is limited by a pinhole, which acts as a spatial filter at the conjugate image plane (confocal plane) positioned directly in front of the photomultiplier. The laser is reflected by a dichromatic mirror and scanned through the specimen in a well-defined focal plane. The emitted fluorescent signals from the sample pass back through the dichromatic mirror and are focused as a confocal point at the detector pinhole aperture. Just a small amount of the emitted fluorescence signal below and above the objective focal plane is delivered through the pinhole aperture, which improves the contrast and also helps to remove background noise. Image of an extended specimen is generated by scanning the focused light- beam across a defined area in a raster pattern controlled by two high-speed oscillating mirrors driven by galvanometer motors. The fluorescence barrier filter before the second pinhole and excitation filter after the light source pinhole aperture helps the separation of the proper wavelength. As an epi-illuminating setup, the single objective lens serve as both the condenser and the objective lens.

Besides creating sharp images of an exact xy-plane of focus, by scanning several focal planes, z-scan is also possible, which means, that the interesting planes can be stacked using a suitable microscopy deconvolution software and analysed as a 3D image which is really helpful for spheroid imaging [71] [72] .

For high resolution confocal imaging, a ZEISS LSM 800 laser scanning confocal microscope (ZEISS, Germany) equipped with HXP 120 V Illuminator (ZEISS, Germany) as fluorescent light source and 10x (ZEISS 10x/0.3 – EC Plan-Neofluar) or 63x oil objective (Zeiss Plan-APOCHROMAT 63X/1.40 oil, ZEISS Germany) was used. The pinhole for data acquisition was set to 1 Airy unit. For image acquisition ZEISS ZEN Microscope Software was used. For image processing, Image J software with core Fiji plugins was used. Brightness and contrast were adjusted, and in case of Z-stack interpretation as an image, stack maximum intensity Z-projection was acquired.

2.2.4.2.   Bright field and epifluorescence microscopy

Leica DMi8 microscope was used to image the formation of spheroids over time and to capture the morphology of the cells in the 6-well plates before process them for Western blotting. The microscope is an inverted microscope equipped with an incubation chamber providing the required temperature and the environment for cell survival. The microscope utilizes the principles of transmitted light microscopy and fluorescent illumination. During transmitted light imaging, the contrast of the specimen is mainly produced by the different absorption levels of light, either due to staining or pigmentation of the specimen. Living cells generally lack natural differences in internal absorption of light, thus the light

traveling through is unable to produce a clearly visible image. Applying additional optical elements, the slight difference or so called intensity phase shift of the specimen and that of the surrounding can be intensified. These phase shifts are converted into changes in amplitude, which can be observed as differences in image contrast [73]. For fluorescent measurements, the implemented filter cubes are swivelled into the beam path by turning the fluorescent turret disk. Time laps imaging with Leica DMi8 (Leica Microsystems) light microscope were performed using 10x phase contrast objective (10x/0.32 PH1 Leica Microsystems). For the fluorescent excitation Leica EL6000 light source was used.

Samples were prepared on 24x60mm cover slides mounted with 20x20mm cover slide using two sided sticky tape and dentist glue (picodent twinsil) for sealing or between two 20x20mm cover slides in small Petri dish which was then covered with FC-40 surfactant mix. For image acquisition Leica Application Suite X software was used. The measurements were conducted at 37°C. For image processing, Image J software with core Fiji plugins was used. Brightness and contrast were adjusted.

2.2.5. Protein quantification by western blot

Protein expression levels were quantified by western blot analysis. Samples were collected at indicated time points. For cell lysis, a lysis mix was prepared from RIPA buffer, with 1% protease inhibitor and 1% EDTA. All possible steps were carried out on ice.

For the 6-well plate experiments, the culturing medium was removed, cells were washed with PBS and treated directly after washing with the lysis mix.

For the 3D culture, the cell suspension was pipetted into a 15 ml tube and centrifuged at 17618 RCF for 5 minutes. The supernatant was discarded and the cells were re-suspended in PBS. The centrifugation step was repeated. The samples were re-suspended in the lysis buffer and transferred to Eppendorfs.
All the samples were gently agitated with the lysis buffer on a horizontal shaker on gentle agitation for 10 minutes. The samples were scraped off the microwell plates, transferred into Eppendorfs and lysated for further 10 minutes on the horizontal shaker. Afterwards, the lysate was centrifuged on 34026 RCF for 15 minutes and either be stored at -20°C or prepared for direct analysis by pipetting the protein containing supernatant off into a new Eppendorf.

The total protein quantity was assessed by Pierce BCA Protein Assay Kit by following manufacturer's instructions (Thermo Fisher Scientific). Protein concentration of the cell lysates were normalized for gel loading.

Before loading, the normalized cell lysates were mixed with RIPA buffer, 10X NuPAGE LDS (Lithium Dodecyl Sulfate) sample buffer and 4X NuPAGE sample reducing buffer mix while diluting them to 1X.

The samples were heated in a sample cooker for 10 minutes at 95°C. After cooking, the samples were placed on ice to cool them quickly, and centrifuged for 30 seconds to collect the content.

For protein separation, Bolt™ 4-12% Bis-Tris Plus polyacrylamide 4-12% gels (Thermo Fisher Scientific/Invitrogen) with 1X dilution of NuPAGE™ MOPS SDS Running buffer (Thermo Fisher Scientific/Invitrogen) (50 mM MOPS, 50 mM Tris Base, 0.1% SDS, 1 mM EDTA, pH 7.7) was used in XCell Surelock Mini electrophoresis chamber (Thermo Fisher Scientific). Electrophoretic separation was performed for 1 h at 200V. After separation, the gel was cracked open, transferred on the top of a sandwich made out of sponges and blotting papers impregnated with running buffer and covered with a nitrocellulose membrane (Invitrogen/Thermo Fisher).

In total, the sandwich consisted of several layers, in the following quantity and order: two sponges, two blotting paper (Thermo Fisher Scientific/Invitrogen, 2.5 mm thick, 7.5 cm x 8.4 cm), the gel, the nitrocellulose membrane, two blotting paper and finally two sponges as shown on **Figure 2.2.2**.

Figure 2.2.2: Blotting stack

The membrane was blotted for 1 hours and 20 minutes on 30 V in the XCell Surelock chamber using 1X dilution of NuPAGE™ Transfer Buffer (Thermo Fisher Scientific/Invitrogen).

Afterwards, the quality of the electrophoresis was assessed by 1% Ponceau S red staining, which was then washed out from the membrane completely with milliQ water.

For blocking before immunofluorescence, the membrane was incubated in 5% BSA (Carl Roth GmbH) in 1x TBS-T, on the horizontal shaker on constant slow agitation for 1 hour on room temperature.

After blocking, the membrane was washed three times with TBS-T for 10 minutes on a horizontal shaker. The membrane was cut into two parts matching the protein sizes to be detected.
Afterwards, the membrane parts were incubated with the primary antibody dilutions as shown in **Table 2.2.3** in 1% BSA (Carl Roth GmbH) in TBS-T and incubated overnight on 4°C.

Subsequently, the membranes were washed three times with 1x TBS-T while agitation on a horizontal shaker for 10 minutes and transferred into the secondary antibody solution (diluted as shown in **Table 2.2.3** 1% BSA (Carl Roth GmbH) in TBS-T). The incubation was performed for 1 hour on room temperature in dark.

Afterwards, the membranes were washed three times with 1x TBST for 10 minutes on horizontal shaker.

If necessary stripping was carried out by following the protocol by Thermo Scientific using Restore Plus Western Blot Stripping Buffer also described by Alegria-Schaffer *et al.* [74].

Subsequently, the fluorescent signal from the secondary antibody was measured with GE Amersham Imager 600. The applied epi white light was filtered at 460 nm wavelength and the emission was detected by Cy2: 525BP20 filter. Images were quantified with Image J with core Fiji plugins using the in-built gel analyzer tool, integrating the localized band intensity curve. The gained β-tubulin values were normalized to the housekeeping protein band intensity values and correlated to the control sample (untreated neuroblastoma cell sample)

Table 2.2.3: Primary and secondary antibodies used in this study

Used antibody	Dilution	Catalog number	Provider
Anti-β -tubulin III	1:4000	T8578	Sigma Aldrich
Anti-β-actin	1:3000	A2668	Sigma Aldrich
Anti-GAPDH	1:4000	MAB374	Merck
Anti-mouse IgG-Alexa488	1:5000	A11001	Invitrogen
Anti-rabbit IgG-Alexa488	1:5000	A11011	Invitrogen

Chapter 3

3.Results

3.1.   Experimental setup assessment

3.1.1. Droplet based microfluidics

Several microfluidic chip with different design were initital assest for the applicability to produce cell cencapsulating droplets. The design varied in their tube diameter (50 µm, 90µm, 100µm), in their inlet filter architecture (no filter, small pore filter, spiral channel, observation chamber) as also seen on **Figure 3.1.1**.
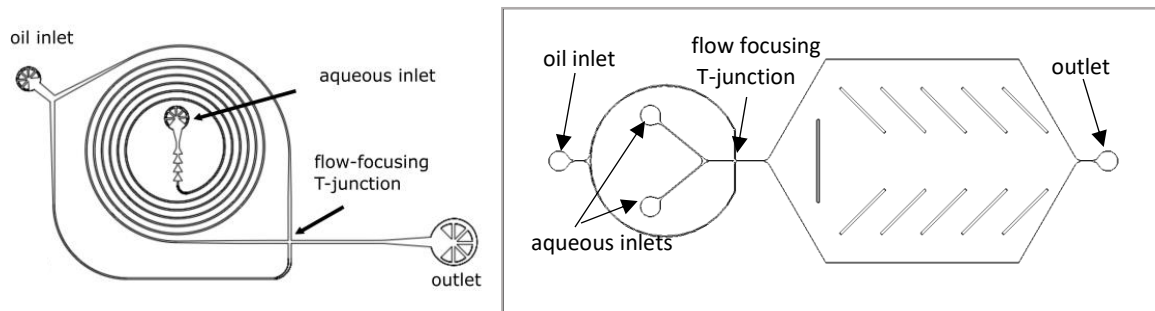

Figure 3.1.1: Design of the deployed microfluidic devices. On the left, a spiral device with 100µm channel size at the T-junction, with small pore filter in silica wafer with lithography without observation channel is shown. On the right, 100µm channel sized device with observation chamber milled into PMMA with CNC machine is shown.

Devices under 100µm channels do not allow the production of sufficiently large droplets under stable and high cell flow rates, and the ones with aqueous inlet filters set back the cell aq. flow by cluster formation. Thus, both of these architectures are disadvantageous for cell confinement. The most stable cell encapsulation was achieved by using 100µm channel diameter devices (shown on **Figure 3.1.2**), and 5(w/v)% Fluorosurfactant in HFE7500. Regarding the injected cell concentration, a minimum of 10 million cell/ml was determined, and a dense cell flow rate was observed at around 20million cell/ml concentration for cell encapsulation for neuroblastoma cells and both natural and the semi-synthetic co-cultures. A relatively slow (roughly ~ 2 droplet/sec, counted manually by visual observation), but

stable droplet production and cell encapsulation was obtained with around 110 mbar pressure applied to the oil inlet and 130 mbar in case of the aqueous phase.
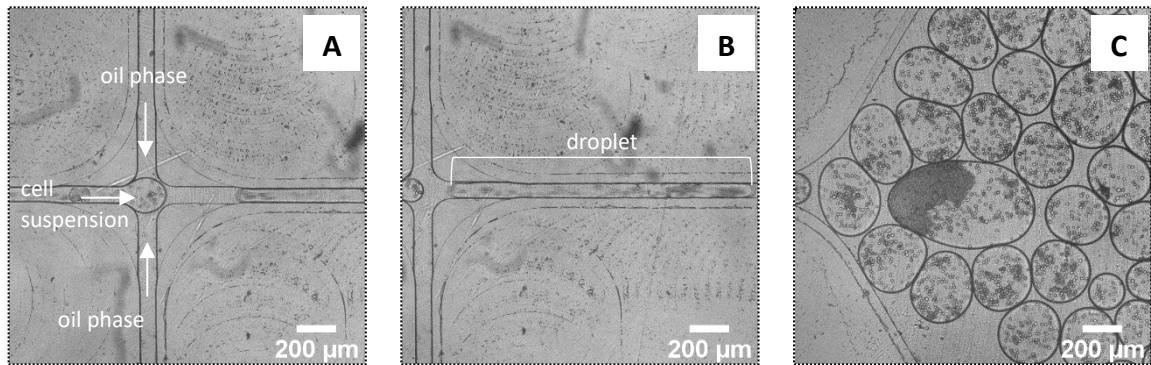

Figure 3.1.2: Cell encapsulation by microfluidic PDMS devices with 100µm channels, using neuroblastoma and astrocyte co-culture with 20 million cell/ml and 5(w/v)% Fluorosurfactant in HFE7500. Image **A** shows the T-junction, where the droplets were formed, picture **B** in the middle shows a droplet cut off, and picture **C** shows the created droplets filled with cells in the observation chamber.

3.1.2. Cell interactions with the surfactant

In the initial testing phase, 1 million cell/ml *HaCat* cells were encapsulated via shaking in droplets **[43]** with surfactant was JW100 in FC-40 (described in section 2.2.1.1 Droplet production). The droplets were observed by confocal microscopy. The Z-stack images showed cell attachment to the droplet periphery along with deformation of the spherical droplet by the cells. Furthermore, the cells showed an elongated or stretched cell body towards each other, shown with arrows on **Figure 3.1.3.** This is not only indicative for successful formation of cell-cell contacts within the droplet but also for excessive attachment to the charged droplet periphery.
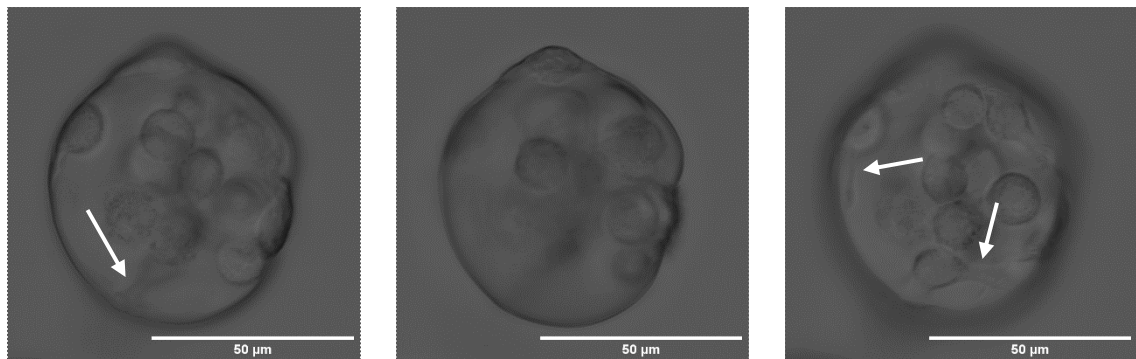

Figure 3.1.3: Confocal microscopy z-stack of *HaCat* cells (1million cell/ml) encapsulated into droplets by shaking method

3.1.3. Cell concentration for spheroid formation

Spheroid formation experiments using spontaneously transformed epithelial *HaCaT* cells were performed to determine an optimal cell concentration for spheroids assembly in droplets by simple shaking method (see section 2.2.1.1 Droplet production).

From images shown in **Figure 3.1.4**, it can be concluded that however all cell concentrations resulted in a packed spheroid-like structure after one day inside the droplets, 5 million cell/ml resulted in the biggest spheroids, among the tested cell concentrations. The created spheroids were in the 50-150μm range.

The HOECHST 33342 and the WGA-AlexaFluor647 staining confirmed intact nuclei, and reasonable cell membrane architectures.
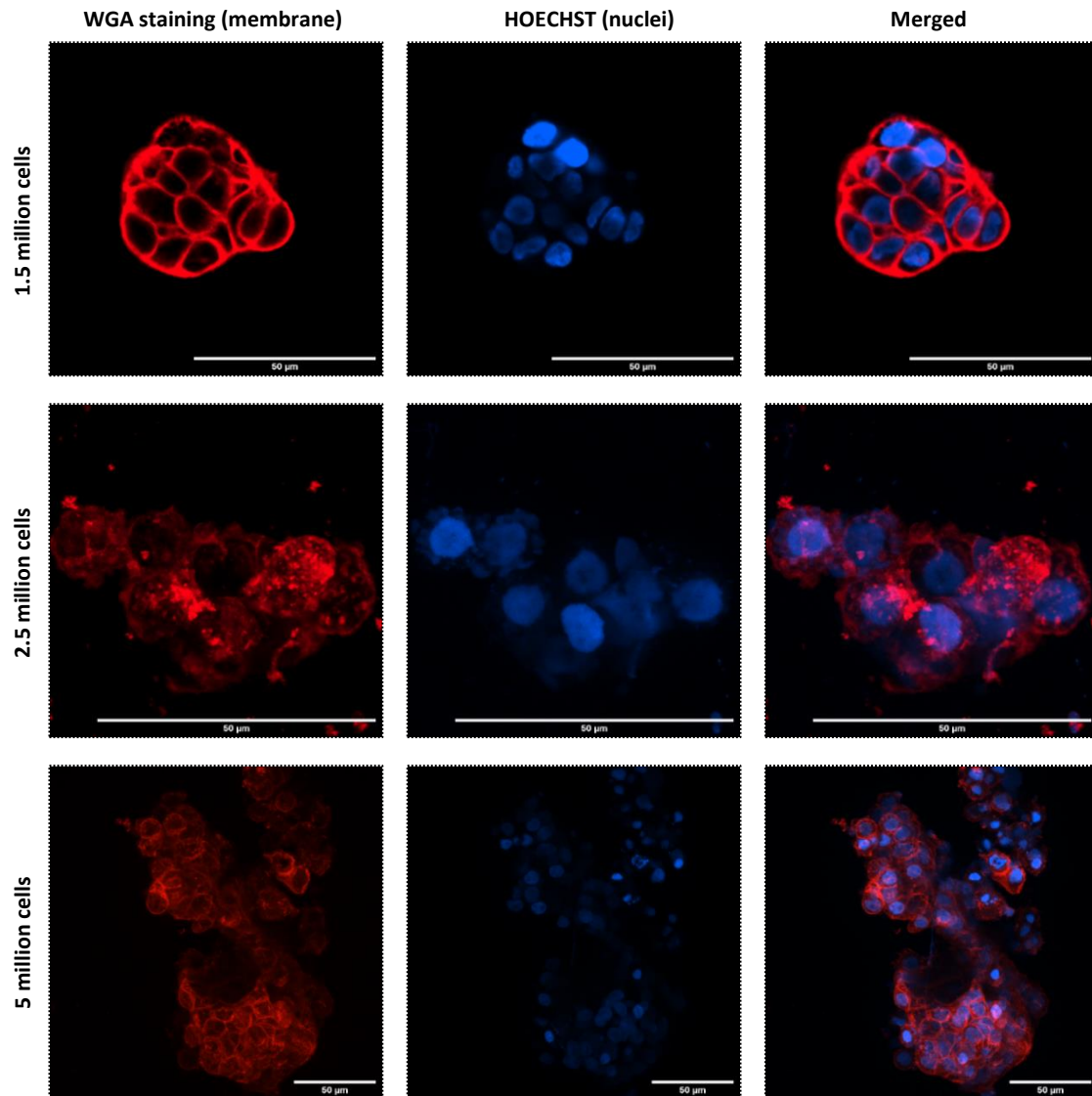
Figure 3.1.4: Confocal microscopy maximal intensity z-projections showing *HaCat* cells (1.5-2.5-5million cell/ml) encapsulated into droplets by shaking method. Cell membrane is stained with WGA-AlexaFluor647 and the nuclei are stained with HOECHST 33342

3.2. Neural and co-culture spheroid generation

3.2.1. Co-cultured spheroid formation

After successful spheroid assembly of *HaCat* cells, neuroblastoma-astrocyte spheroids were formed as a proof of concept. Using separate CellTracker blue and green staining, neuroblastoma and astrocytes could be distinguished inside the droplet and the distribution and combination of the separate cell types could been followed as seen in **Figure 3.2.1**. The droplets were produced by microfluidics, using 2.5mM JW100 surfactant in FC-40. The used cell concentration was 2.5 million cell/ml in total, and a resulting 200μm spheroid size could be measured after 14.5 hours of incubation. The cells fully aggregated after approximately 7 hours. The cell types mixed during the spheroid formation, no preferential single cell-type clusters were observed.
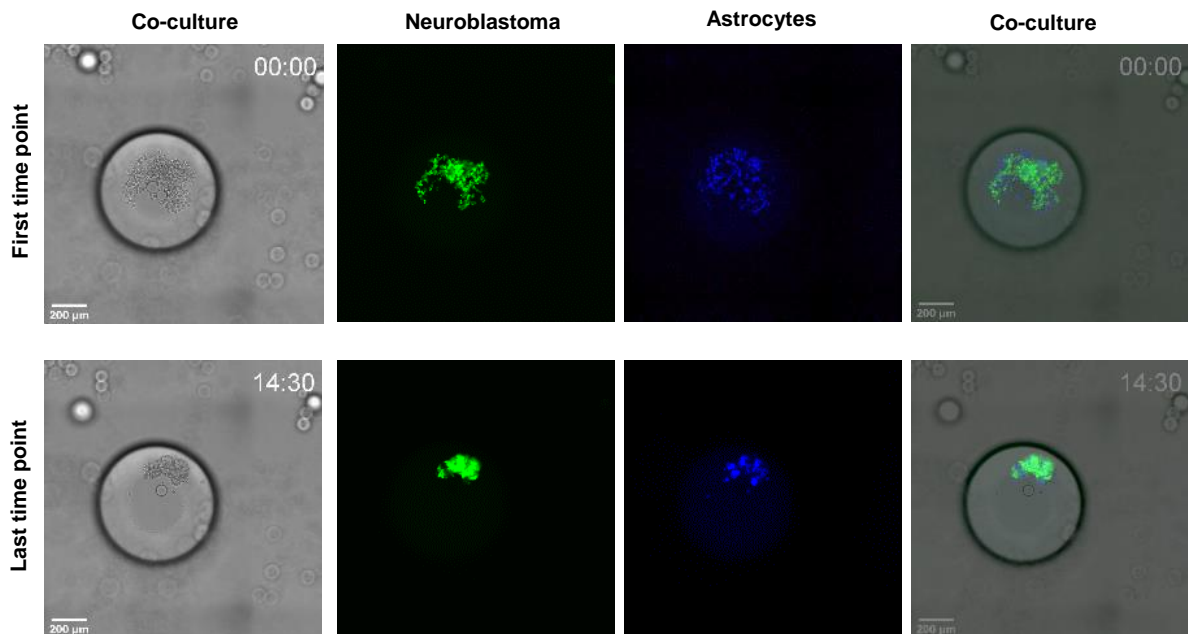
Figure 3.2.1: Time laps observation of spheroid formation. From left to right: Phase contrast image of the co-culture; neuroblastoma cells (*SH-SY5Y*) - stained with CellTracker green CMFDA; astrocytes (*HS683*) - CellTracker blue CMAC; merged image of the stained co-culture inside the droplet. First row depicts the status at time point zero, the second row shows the end result after 14.5 hours of incubation.

3.2.2. Immunofluorescent detection of differentiation

Neuroblastoma and neuroblastoma-astrocyte co-culture spheroids were formed inside of droplets by shaking method as well as using microfluidic device (see sections 2.2.3.2.Cell release, fixing and staining & 2.2.1.1 Droplet production) to compare the efficacy of the spheroid formation of these methods as well as the survival of the cells during the separate methods. The assembled spheroids were released from the droplets after 1 day. The spheroids produced via microfluidic devices were more concise and uniform compared to the ones created with the shaking method. The immunofluorescent staining showed a distinct signal, thus indicating neural maturation in the confinement. In all cases, the created spheroids were in the 50µm range. The nucleus staining show intact nuclei and in some cases a division process was observed.
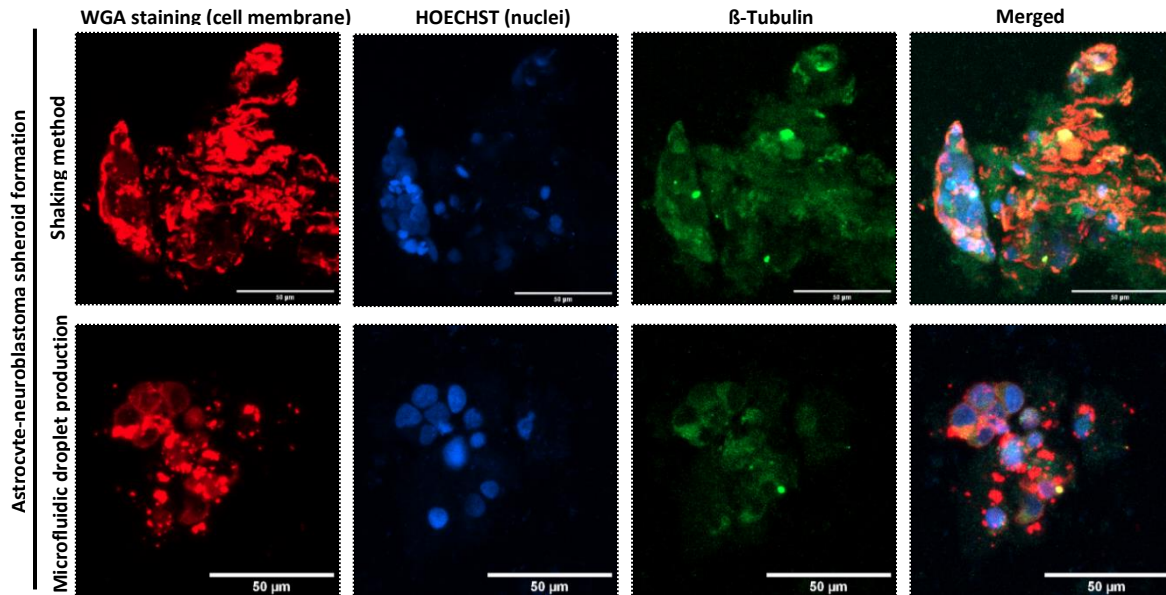

Figure 3.2.2: Fluorescence confocal microscopy maximal intensity z-projections of neuroblastoma-astrocyte co-culture spheroid formation with droplet based microfluidics and shaking method. Immunofluorescent labelling performed using β-tubulin and anti-mouse IgG-Alexa488, the cell membrane was visualised with WGA-AlexaFluor647, the nuclei was stained with HOECHST 334342. The method of the spheroid formation as well as the type of spheroid generated is indicated on the left side of the images.
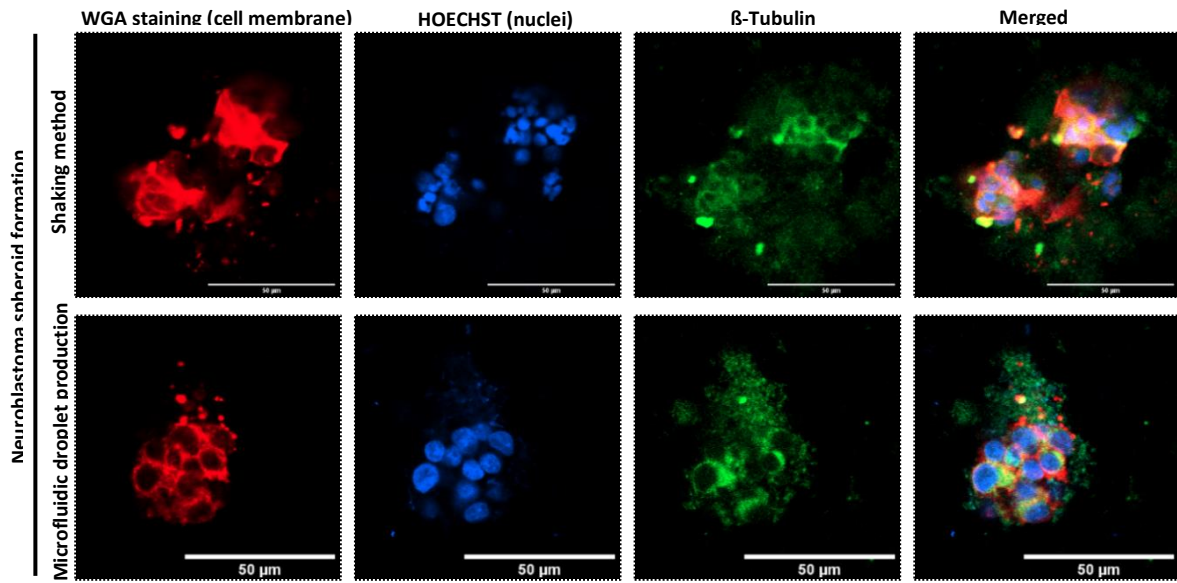
Figure 3.2.3: Fluorescence confocal microscopy maximal intensity z-projections of neural spheroid formation with droplet based microfluidics and shaking method. Immunofluorescent labelling performed using β-tubulin and anti-mouse IgG-Alexa488, the cell membrane was visualised with WGA-AlexaFluor647, the nuclei were stained with HOECHST 334342. The method of the spheroid formation as well as the type of spheroid generated is indicated on the left side of the figures.

3.2.3. Incorporation of synthetic cell into the spheroids

After successful spheroid generation, GUV incorporation into spheroids was tested. As a proof of concept, GUVs without NrCAM ligand, but with 1% NTA tagged and negatively charged lipids (20% negatively charged EggPG, 78% EggPC, 1% LissRhod **Table 2.2.2**)were introduced to the cells in bulk. For this experiment, 8 million neuroblastoma cells in 10 ml culturing media were incubated in a non-adherent flask for 7 days. As **Figure 3.2.4** shows, GUVs are attaching to the neuroblastoma spheroids.
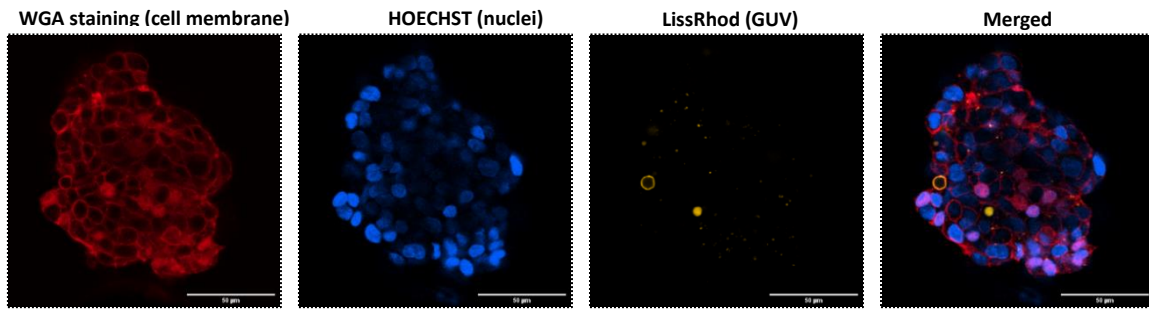
Figure 3.2.4: Fluorescence confocal microscopy single plane image of neuronal spheroids produced in non-adherent flask, incorporating GUVs with negative charge and NTA-tag. The cell membranes was stained with WGA-AlexaFluor647, the nuclei were stained with HOECHST 334342 and the GUVs are visualized utilizing the LissRhod lipid composites. The showed spheroid is around 100μm.

Subsequently, neuroblastoma cells ($2.5*10^5$ cell/ml cell concentration) were incubated together with the minimal synthetic astrocytes: NrCAM biofunctionalized GUVs in 15 ml falcon tube (bulk) for 7 days, the results is shown on **Figure 3.2.5**. These GUVs were composed of 1%NTA, 20% EggPG, 78% EggPC, and 1% LissRhod. Towards this end, the NrCAM quantity was adjusted to match the molarity of the NTA-tagged lipids in the GUV composition.
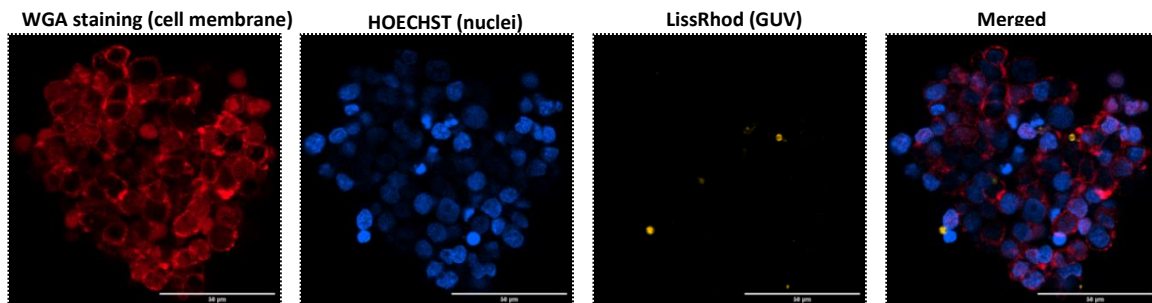

Figure 3.2.5: Fluorescence confocal microscopy single plane image of semi-synthetic spheroid in bulk, grown for 7 days, in 100μm size range. The cell membranes was stained with WGA-AlexaFluor647, the nuclei were stained with HOECHST 334342 and the GUVs are visualized utilizing the LissRhod lipid composites.

3.3. Functional and morphological assessment

3.3.1. 2D morphological assessments

In order to opbtain a positiv control for neuronal differentiation, we tested the effect of different ratios of retinoic acid. As previous reports have shown previously [7][12], 10µM concentration resulted in the most extended axonal projections connecting neighbouring cells and neuron-like elongated cell bodies as shown on **Figure 3.3.1** on the left. For this assessment, $2.5 *10^5$cell/ml concentration was used.
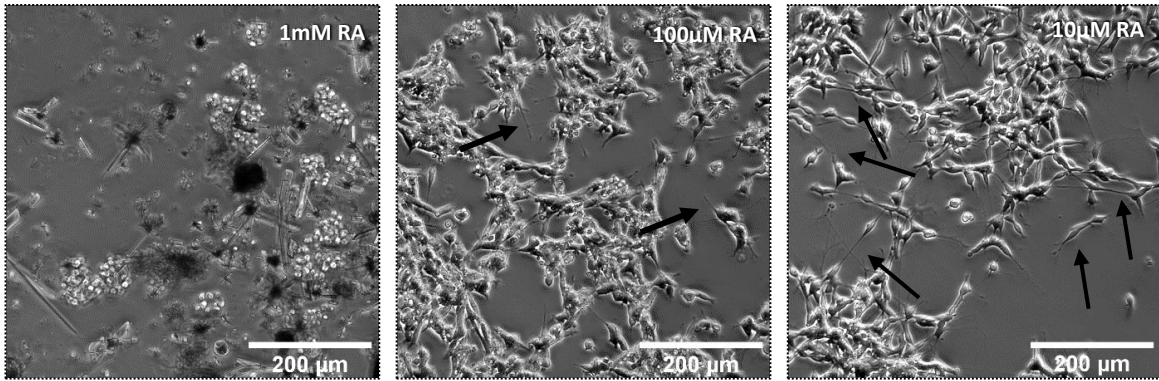

Figure 3.3.1: Phase contrast images of *SH-SY5Y* 2D cell cultures for morphological assessment of the effect of three different concentrations of RA on neuroblastoma cells in 2D cell culture, 7 days after incubation.

Effect on neuroblastoma (*SH-SY5Y*) morphology of different GUV concentration was investigated on 2D culture morphology, using $2.5*10^5$ cell/ml (**Figure 3.3.2**). There was no significant morphological difference found between neuroblastoma cultures supplemented with different unfunctionalized GUV concentrations and untreated cultures.
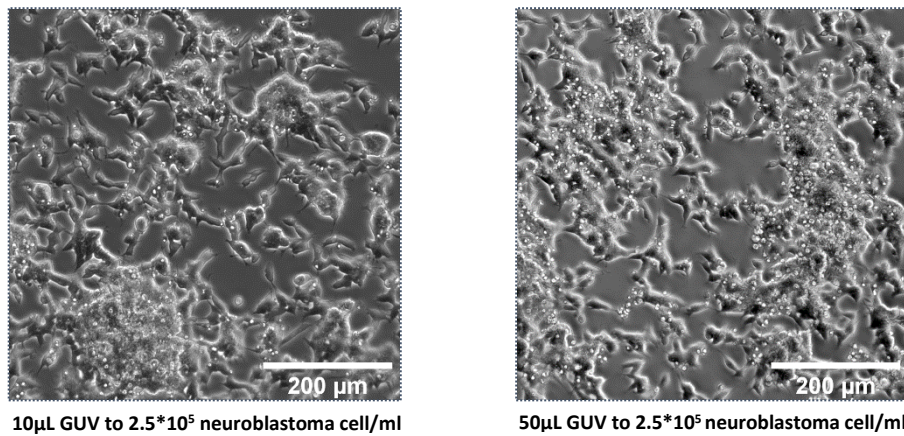

10µL GUV to $2.5*10^5$ neuroblastoma cell/ml   50µL GUV to $2.5*10^5$ neuroblastoma cell/ml

Figure 3.3.2: Phase contrast images of *SH-SY5Y* 2D cell cultures for morphological assessment of increasing concentrations of GUV incubated with the neuroblastoma cells after 7 days of incubation.

The cell morphology of in response to NrCAM was evaluated as introduced on **Figure 3.3.3**. In one condition only NrCAM was added to the media in soluble form, and NrCAM immobilized on the GUV surface via His-Tag chemistry. The morphology of both NrCAM supplemented cell cultures showed an increased axonal cell connectivity and stretched cell morphology which is characteristic to neuronal cells. In all cases, cells appear to be viable.
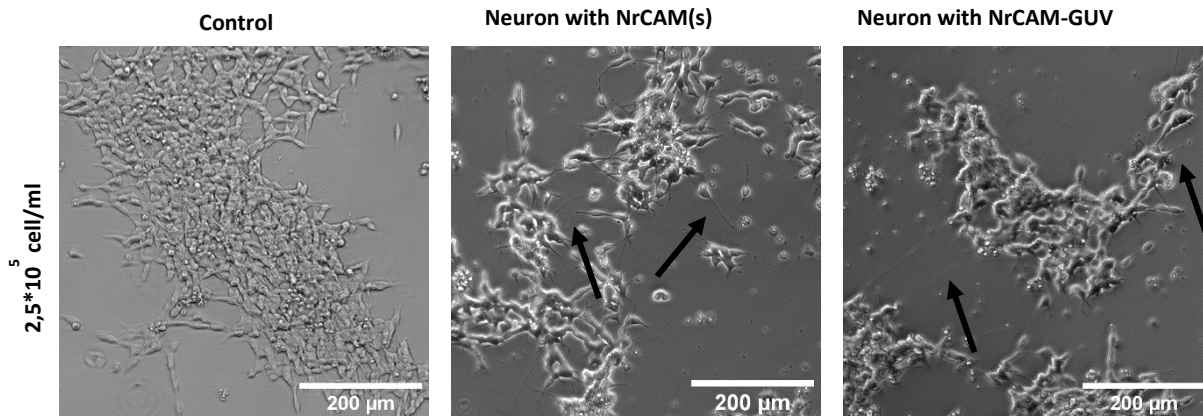

Figure 3.3.3: Phase contrast images of *SH-SY5Y* 2D cell cultures for morphological response of neuroblastoma cells to soluble and GUV- bound (minimal synthetic astrocyte) form of NrCAM molecule after 7 days of incubation.

A higher cell concentration (25 million cell/ml) of neuroblastoma cells was incubated in 2D culture with the soluble form of NrCAM, GUV-bound NrCAM to test morphological differences. Furthermore, to optimize the NrCAM and NrCAM-GUV concentration, 10-times less concentration of each was also introduced to the cell cultures. In all cases, cells were treated with retinoic acid to kick-start the differentiation process. After 7 days of incubation, there is only slight visible difference in the means of morphology, as presented on **Figure 3.3.4**.
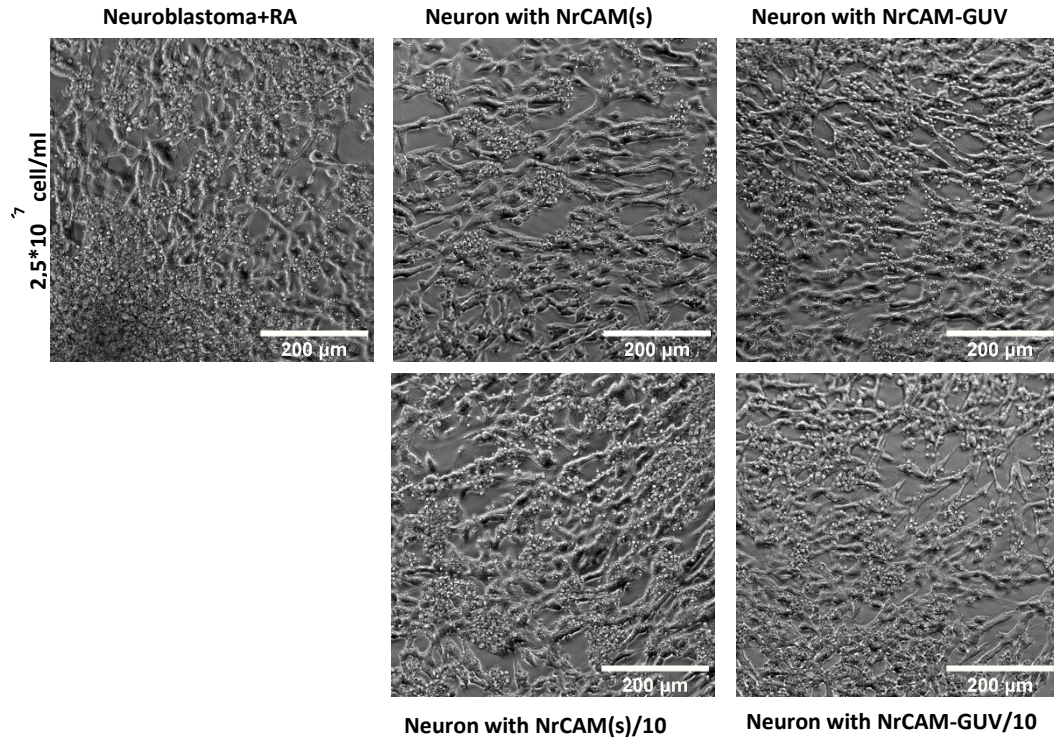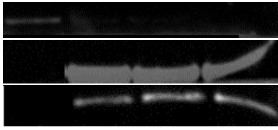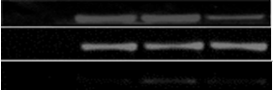
Figure 3.3.4: Phase contrast images of *SH-SY5Y* 2D cell cultures for morphological response of 25million cell/ml neuroblastoma cells incubated for 7 days with soluble form of NrCAM, NrCAM-GUVs, and 10-times lower concentration of NrCAM, NrCAM-GUVs. Retinoic acid was used in all cases to kick-start differentiation.

3.3.2. Functional assessment by Western blot analysis

An western-blot setup to quantify differentiation by the signal intensity of the expression marker signals was established. The used differentiation marker was first β-actin, later on β-tubulin.

Effect of retinoic acid on neuroblastoma cells at three time points was assessed by western blot. 3µg of total protein was used for the measurements. On day 1, in the 2D system, the integrated relative signal values do not reach that of the control group, which was the untreated neuroblastoma cell samples. Furthermore, there is a large variability between different time points and concentrations. Normalization was not available, due to the low signal of β-actin.

Table 3.3.1: Effect of different concentration of retinoic acid on neuroblastoma (*SH-SY5Y*) cells on day 1-3-7 in 2D and 3D cultures. Integrated values, relative to the signal of the control cells, the values are not normalized. Red shows the values lower than the signal of the control sample. Bands are shown next to the condition, respectively.

	Retinoic acid concentration			
2D system	**1mM**	**100µM**	**10µM**	
Day1	0.007	0.231	0.454	2D-Day1
Day3	3680.870	4117.301	18263.569	2D-Day2
Day7	46.508	48.819	30.356	2D-Day3

3D system	**1mM**	**100µM**	**10µM**	
Day1	135.025	118.063	205.096	3D-Day1
Day3	1007.148	897.830	909.691	3D-Day2
Day7	160.340	282.510	67.970	3D-Day3

The ability to induce differentiation of neuroblastoma cells by NrCAM was assessed by western blotting. In four parallel measurements, the NrCAM in soluble form in the cell culturing media, in molar balance to the NTA-tagged lipid composite in the GUVs was measured. For this a standard curve was fitted and the theoretical binding capacity was calculated. In the followings, the calculation for determining the NrCAM concentration needed is shown:

Calculcation:

- Translation of NrCAM concentration to molar concentration:

NrCAM $500\frac{\mu g}{ml}$, MW= 67kDa ~$67000\frac{g}{mol}$

$c = \frac{n}{V} = 7.46\mu M$

- <u>Theoretical</u> NTA lipid concentration (1% NTA tagged lipid)

$c_{(lipid)_{total}}$=6000µM=6mM, $V_{(lipid)_{total}}$= 300µL   (**Table 2.2.2**)

$c_{(lipid)_{NTA}}$=1%*6000µM=60µM

Neglecting all the losses during GUV production, the lipid solution was diluted 1:1, with final total concentrations:

$c_{(lipid)_{total}}$=3000µM=3mM, $V_{(lipid)_{total}}$= 600µL

$c_{(lipid)_{NTA}}$=1%*3000µM=30µM

30 µmol	in	1L
x	in	600µL

$$\frac{600µL}{1000000µL} \times 30\ µmol = 0,018µmol\ \left(n_{(NTA\text{-}lipid)}\right)$$

- We assumed 10% release efficacy, accordingly:

$n_{(NTA\text{-}lipid)}$ =0,018µmol *0,1= 0.0018µmol = 1.8nmol

- First, 40µL of NrCAM was coupled to the NTA-GUVs:

1.8 nmol	in	600µL
x	in	40µL

$$\frac{40µL}{600µL} \times 1.8\ µmol = 0.12nmol\ \left(n_{(NTA\text{-}lipid)}\right)$$

- To provide $n_{(NTA\text{-}lipid)} = n_{(NrCAM)}$ molar equilibrium:

7.46 µmol=7460nmol	in	1000mL
0.12 nmol	in	xµL

$$\frac{0.12\ nmol}{7460\ nmol} \times 1000\ mL = 0.016mL = 16µL \qquad \left(n_{(NrCAM)}\right)$$

For the <u>experimental</u> NTA-lipid concentration, a GUV standard curve was fitted. Two measurement patterns were used, which resulted in slight different values in the absrobance of the standard samples. The values were averaged for each concentration, and two standard curves were set up and equations were fitted:

GUV abs. before cleaning

GUV abs. after cleaning

$$y = 13.586x + 611.87; \quad R^2 = 0.9972 \qquad y = 1.2207x + 68.2; \quad R^2 = 0.9985$$
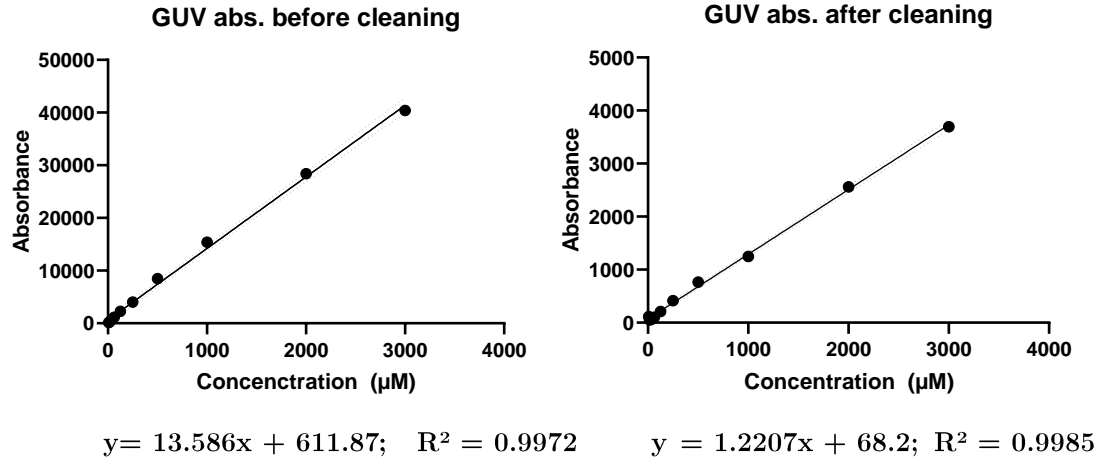
The NTA-GUV samples were measured with the same patterns as well as gains, resulting in average absorbances:

$$A_{gain\ 78}(585nm)_{NTA\text{-}GUV} = 13926.67\ nm \qquad A_{gain\ 76}(585nm)_{NTA\text{-}GUV} = 11701\ nm$$

According to this, the NTA-GUV only fitted into the "GUV abs. before cleaning" curve.

$$x = \frac{13926.67}{13.586} - 611.87 = 412.87 \mu M$$

If $c(lipid)_{NTA} = 30 \mu M$ in $c(lipid)_{total} = 3000 \mu M$, then

in $c_1(lipid)_{total} = 412.87\ \mu M$ - $c_1(lipid)_{NTA} = 4.13\ \mu M$ and

- For curve fitting, 75 µL was used

4.13 µmol	in	1 L
x	in	75µL

$$\frac{75 \mu L}{1000000 \mu L} \times 4.13\ \mu mol = 309.75 pmol\ \left(n_{(NTA\text{-}lipid)}\right)$$

This shows the molar amount of the assumed NTA-tags on the GUV lipid membrane available. As an example, required NrCAM volume can be calculated for this NTA amount as followings:

0.12 nmol	in	16µL
309.75 pmol	in	xµL

$$\frac{0.12 nmol}{0.30975\ nmol} \times 16 \mu L = 6.2\ \mu L\ (V_{NrCAM})$$

The GAPDH normalized β-tubulin values are related to the NrCAM GUVs and the media dissolved NrCAM values were collected into **Table 3.3.2**. It can be observed, that in case of the 2D, half of the positive controls' and one samples' signal did not reach the level of that of the negative control. In case of the 3D samples, three in media dispersed NrCAM sample and two GUV bound sample exceed the signal of the positive control.

Table 3.3.2: GAPDH normalized relative beta tubulin values. Red shows the values lower than the signal of the control sample.

3D system	GAPDH normalized relative tubulin values			
Negative control	1	1	1	1
Positive control	6.78054778	0.22534335	1.00999728	1.92431737
Neurons:NrCAM(s)	7.43979787	5.91334875	0.77984657	1.83155737
Neurons:NrCAM-GUV	1.20699134	0.33858358	0.88732053	1.650619
Neurons:Astrocytes 1:1	0.13628738	0.00153956	0.07946133	0.06266392

2D system	GAPDH normalized relative tubulin values			
Negative control	1	1	1	1
Positive control	0.0689759	0.92556356	1.77218171	1.7640615
Neurons:NrCAM(s)	0.02879246	0.86164783	0.96175758	0.85848154
Neurons:NrCAM-GUV	0.0488799	0.81145949	1.01740853	0.79593297
Neurons:Astrocytes 1:1	0.00051007	0.00012322	0.05038171	0.03112604

The GAPDH normalized β-tubulin values are shown in **Figure 3.3.5, Figure 3.3.6, Figure 3.3.7** and **Figure 3.3.8.** Respective bands of the processed and presented results are shown above the diagram, bands were analysed with ImageJ gel analyser tool. The acquired data varies a significantky and the housekeeping protein expression signal presented by the astrocyte containing sample is high in all cases. In general, β-tubulin values of the 2D samples appear at 2-3-fold more intensive, however their normalized values are lower or comparable to that of the 3D samples.

On Figure 3.3.5 e very intensive β-tubulin signals in case of the 2D samples can be seen, however when normalizing them to the housekeeping protein and correlating them to the negative control, the signals are almost 0. In comparison, for the 3D samples on the same figure, the highest positive control and media solved NrCAM values can be seen.

Signals of the 2D samples on Figure 3.3.7 and Figure 3.3.8 appear with similar intensity. However, the 3D measurement of the same set of samples, when comparing them to each other, only values on Figure 3.3.8 are stronger than the negative control signal value, if signals coming from the samples with the astrocytes are neglected.
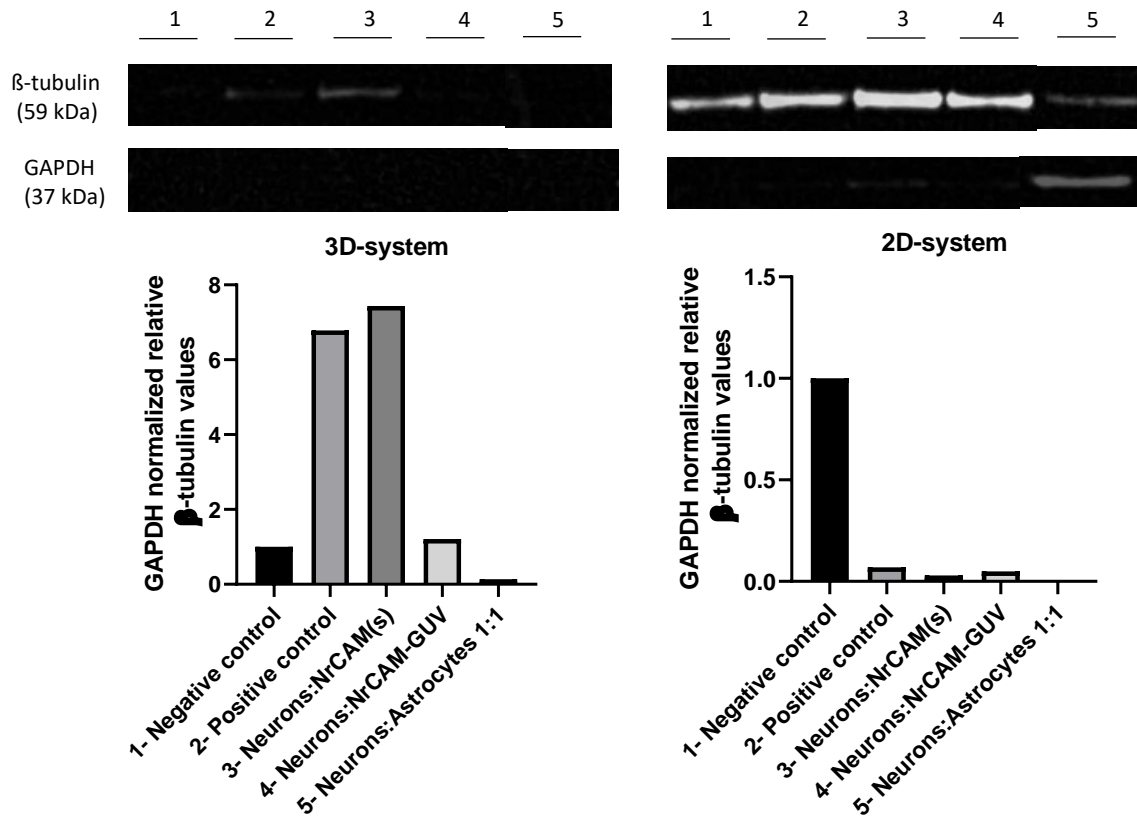
Figure 3.3.5: GAPDH normalized relative β-tubulin values. Respective bands are shown above the diagram, bands were analysed with ImageJ gel analyzer tool. Numbers over the bands corresponds to the numbered description under the diagram.
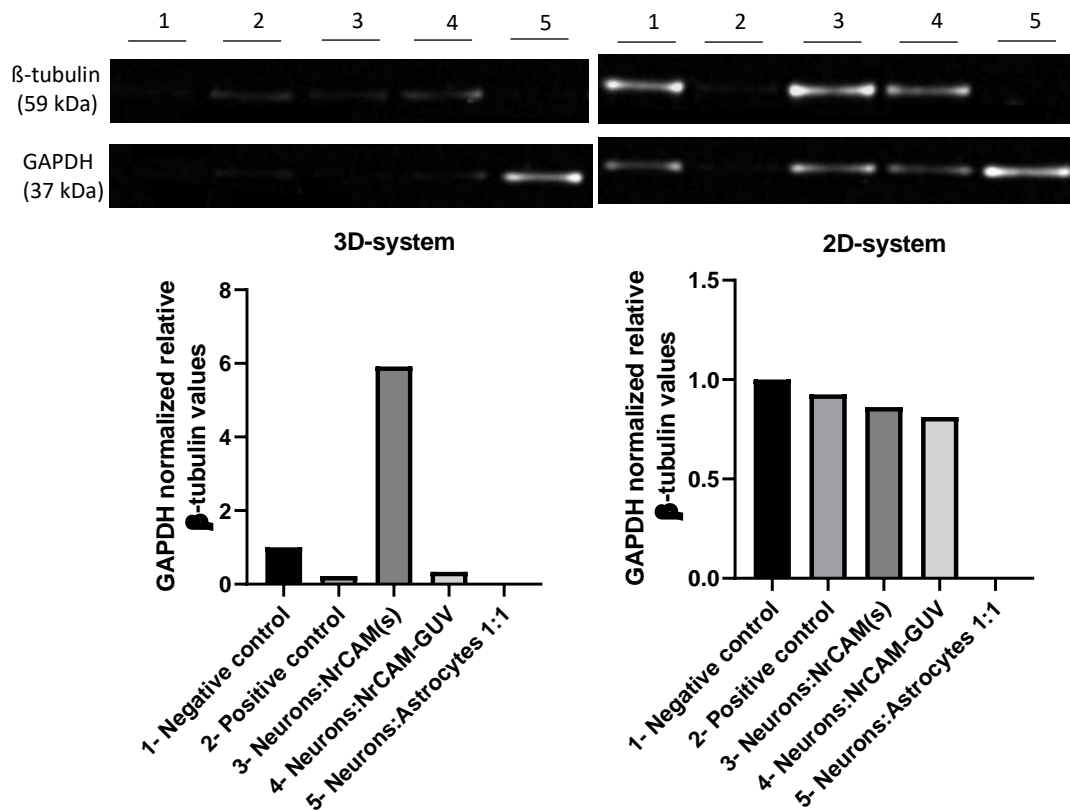

Figure 3.3.6: GAPDH normalized relative β-tubulin values Respective bands are shown above the diagram, bands were analysed with ImageJ gel analyzer tool. Numbers over the bands corresponds to the numbered description under the diagram.
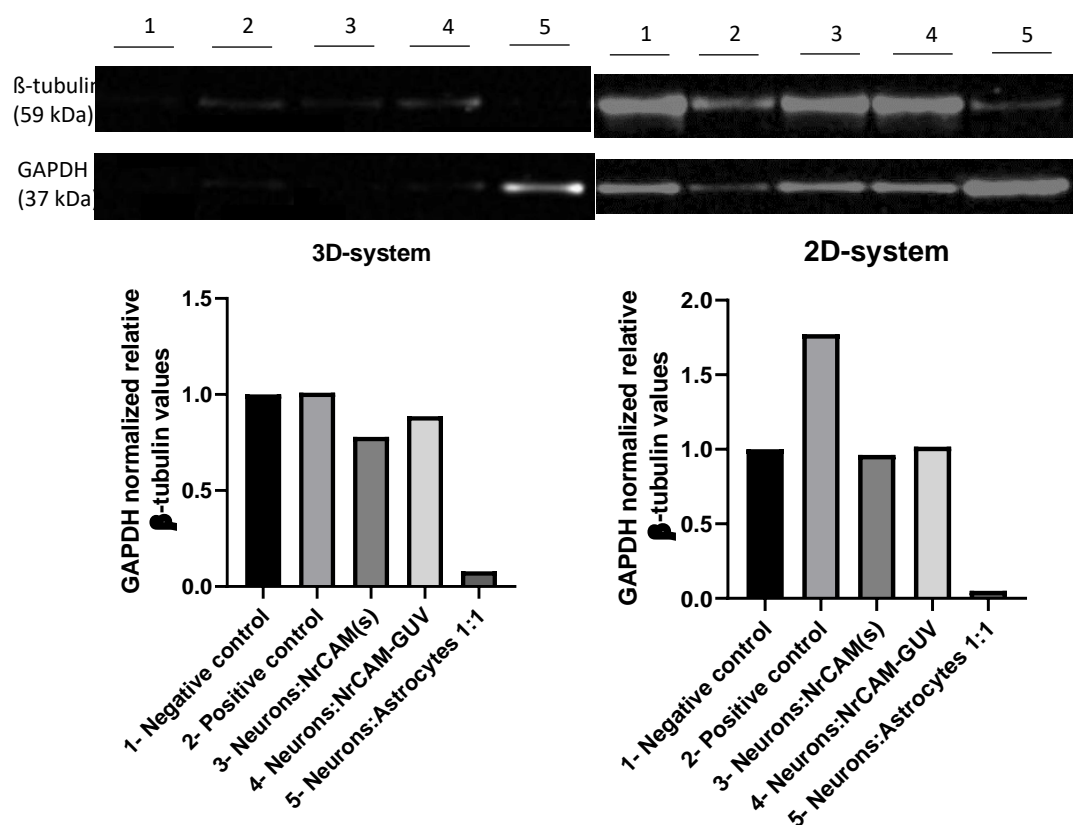
Figure 3.3.7: GAPDH normalized relative β-tubulin values Respective bands are shown above the diagram, bands were analysed with ImageJ gel analyzer tool. Numbers over the bands corresponds to the numbered description under the diagram.

Figure 3.3.8: GAPDH normalized relative β-tubulin values Respective bands are shown above the diagram, bands were analysed with ImageJ gel analyzer tool. Numbers over the bands corresponds to the numbered description under the diagram. values
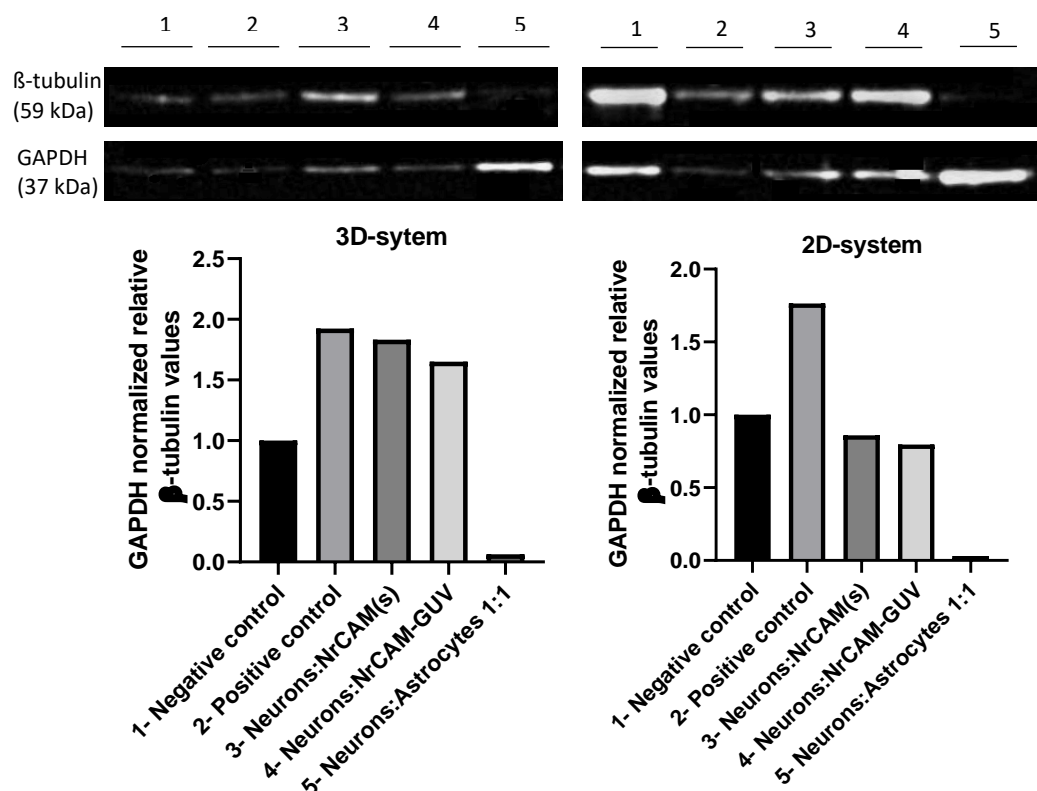
Chapter 4

4.Discussion

The here demonstrated attachment of the *HaCat* cells to the droplet periphery on **Figure 3.1.3** can be explained by the characteristics of the used surfactant. JW100 is an in house synthesized surfactant, which due to the steps of the synthesis, inevitably contains carboxylic residues, and hence a negative charge in the aq. droplet environment. This is favourable for the cells as in this way they attach to the droplet charged droplet periphery [66]. Furthermore, the cells showed an elongation and spreading towards each other (shown with arrows on **Figure 3.1.3**), which is also indicative for a healthy cell population.

The preliminary *HaCat* assessment also showed that a minimum concentration of 5 million cell/ml would result in the largest spheroid size, at least in case of the shaking method shown by **Figure 3.1.4**. These experiment also proof that cells form spheroid and most importantly survive for at least one day.

Analysis of the time laps observation revealing the formation of neuroblastoma-astrocyte spheroids shown on **Figure 3.2.1,** revealed a relatively quick spheroid generation. During transfer of the droplet to the observation chamber, fusion of the droplets was observed. However 70% of the surviving droplets at the starting point of the time laps in the observed area remained intact during the observation period. It was concluded, that a specific fluorosurfactant concentration and composition is needed to promote and stabilize the in droplet spheroid formation, especially if the droplets need to be transferred between different production and observation setups.

Figure 3.2.4 shows an incorporation of non-functionalised GUV into the neuroblastoma spheroids. This can be explained by the charge present on the GUV due to the presence of charged EggPG lipids in the GUV membrane. This result is a proof of principle for the incorporation of synthetic vesicles into a neural spheroid without disruption the intrinsic 3D cellular assembly. When NrCAM functionalized GUVs were incorporated into the neuroblastoma spheroids, no significant change in the spheroidal assembly was observed. As a next step the quantity of incorporated GUVs needs to be increased, to more accurately mimic the in-vivo astrocytes-to-neuron ratio and therefore to provide a comparable native environment for differentiation. In future, the size and the stiffness of the GUVs could be

modified to elevate the functional response and the phenotypic attributes of the created spheroids.

When assessing the influence of retinoic acid concertation on β-tubulin expression, 1mM showed a comparable response to 100µM and to t 10µM (see **Table 3.3.1)** This is indicative for successful differentiation and maturation. However, at 1mM RA, cells appeared with unhealthy morphologies. This effect might be attributed to cell toxicity due to the high DMSO concentration used (RA was diluted in DMSO). 10µM on the other hand, showed the best morphological comparability to mature neuronal cells which is shown on **Figure 3.3.1** and in most cases the differential protein expression marker had the strongest signal intensity among all (compare **Table 3.3.1)**. This result are in accordance to literature reports where 10µM RA was used to differentiate *SH-SY5Y* neuroblastoma cells within 7 days. 2.5 *10^5cell/ml concentration was used based on Cheung *et al,* where 2*10^5 cell/ well were treated in 6-well plates [12] .

Due to time restrictions, the results of the functional assessment by wester blotting still needs to be adjusted, nevertheless some conclusions and tendencies can be appreciated. For the quantitative assessment by western blotting, originally β-actin staining was chosen as an expression reference housekeeping gene. However, the staining performed inconsequently and with a very low signal. Consequently the signals acquired from the retinoic acid optimization could not be normalized, and thus cannot be scientifically approved. Importantly, Castaño *et al* [75] reported that β- actin as internal control, leads to an underestimation of the levels of other protein(s) in for differentiated *SH-SY5Y* cells. Based on this report, the recommended housekeeping expression marker GAPDH was further used. Indeed, a more comparable and stable signal to the β-actin signal was found. Therefore, the presented quantifications still need to be verified, despite the presence of a clear tendency towards an increased differentiation in contact with 10µM retinoic acid.

When looking at the NrCAM-induced differentiation in **Table 3.3.2**, the soluble NrCAM induces in three out of four trials a higher differention marker expression compared to the GUV bound form. This can be explained by the instant availability of the NrCAM in the cell media. The cells might be triggered more efficiently by the ambient presence of NrCAM. Whereas in case of the GUV bound, it requires and inevitable contact between the cells and the GUVs. This might results in a slowed down kinetic, since in this case, the GUVs first need to diffuse and establish the contact. Maybe, once formed, the differentiation processes will be more efficiently, as the local NrCAM concentration on the GUV membrane will be several orders of magnitude higher compared to the soluble form. For this purpose, in-droplet droplet incubation and differentiation might increase the response as they provide a confined space for GUV-spheroid contact formation. The conclusion derived from these experiments are that NrCAM in general induced differentiation on a higher extent in 3D, in some cases

even exceeding the differentiation induced by RA. It can be observed, that in the case of 2D cultures, half of the positive controls' and the samples' signal did not reach the intensity of the negative control. This is indicative for a systematic failure of the respective experiments.

As mentioned previously, the adjustment and optimization of the NrCAM-GUV concentration as well as the western blot imaging signals is still ongoing considering that the astrocyte-neuroblastoma broadcasted housekeeping protein expression signal was too high. In conclusion, this shows that astrocytes possess a high GAPDH expression, rendering their assessment and contribution in this quantification protocol inappropiate.

Microfluidic preparation of spheroids was performed for western blotting. The samples´ β-tubulin signal was unfortunately not detectable in any case. The most apparent reason was that the samples contained a very limited amount of protein during total protein quantification. This means first of all, that the prepared sample size was not sufficient even if we consider the higher cell concentration used for microfluidic droplet production. Another possible explanation is that the cells were excessively shocked during the production, which shut certain expression down. In the future, increased sample volumes need to be produced in order to decipher the possible breaking points of the experiment. As shown shown in **Figure 3.2.2** and **Figure 3.2.3**, spheroids form and survive for one day inside of droplets and even endure a whole staining process. Accordingly, one other speculated vulnerability of the cells is the incubation after the release.

The GAPDH normalized β-tubulin values shown in **Figure 3.3.5, Figure 3.3.6, Figure 3.3.7** and **Figure 3.3.8** are presented in chronological order. The signals on **Figure 3.3.7** and **Figure 3.3.8** are in a comparable range of 0.5-2 unit which suggests that the analysis improved.

Another differentiation marker, fyn-kinase, was tested in a prelaminar phase, experimental procedure for its assessment requires further optimization. Moreover, in the future, the stripping method of the blotting membranes and the housekeeping protein expression has to be optimized for astrocyte containing samples.

Chapter 5

5.Conclusion

In summary, single cell line and co-culture spheroids can be assembled in droplets produced in microfluidic channels and also by a simple shaking method[43] . In case of microfluidic production, the diameter of the channels has to reach 100µm in order to create 50-150µm sized spheroids. Uncharged surfactant is necessary in order to avoid cell attachment to the droplet periphery, 5%(w/v) Fluorosurfactant in HFE7500 provided the best stability to encapsulate cell culture and co-culture. The cell concentration to form co-cultured spheroids was concluded to be optimal between a minimum of $10*10^6$ cell/ml to $25*10^6$ cell/ml. Co-cultured spheroid formation can be followed by staining the separate cell lines, and spheroids were shown to form after 7 hours. Spheroids appear viable after release, fixing and staining.

GUVs can be incorporated into spheroids, essentially due to their charge and no specific protein-protein interactions seem to be needed. The co-culturing with GUV does not disrupt the natural cell assembly and the cells in the formed spheroid seem to be intact by means of their morphology.

Differentiation marker quantification by a western blotting method was established to analyse the functional response by means of differentiation of neuroblastoma cells to different treatments. For this purpose, β-tubulin served as a good expression marker for differentiation, and as a housekeeping protein, GAPDH emerged as the optimal choice.

10µM retinoic acid concentration high potency to kick-start differentiation in *SH-SY5Y* neuroblastoma cells. Therefor, RA treated samples were chosen to be used as a potential positive control for further differentiation assays. This property was confirmed by morphological assessment. The functional assay also suggested an increased differentiation for cultures treated with 10µM RA. However the signals could not be normalized to a proper housekeeping gene at this stage of the study, wherefore these results need to be re-evaluated.

NrCAM functionalized GUVs were evaluated to act as astrocyte-mimics in neuroblastoma-astrocyte spheroids due to the prevalence of NrCAM on the cell membrane of astrocytes. NrCAM was hypothesized to induce differentiation in neuroblastoma cells after adhesion. At this stage, this hypothesis cannot be proved, due to the faults of the fluorescence imaging in western blot analysis. However, the functional assessment suggested that the NrCAM, especially NrCAM dissolved in media, induces differentiation of 3D neuroblastoma spheroids.

Further evaluation need to confirm this assumption for statistical significance. Differentiation within droplet stabilized spheroid could not be detected.

List of figures and tables

Figure 3.3.1: Phase contrast images of *SH-SY5Y* 2D cell cultures for morphological assessment of the effect of three different concentrations of RA on neuroblastoma cells in 2D cell culture, 7 days after incubation.

Figure 3.3.2: Phase contrast images of *SH-SY5Y* 2D cell cultures for morphological assessment of increasing concentrations of GUV incubated with the neuroblastoma cells after 7 days of incubation.

Figure 3.3.3: Phase contrast images of *SH-SY5Y* 2D cell cultures for morphological response of neuroblastoma cells to soluble and GUV- bound (minimal synthetic astrocyte) form of NrCAM molecule after 7 days of incubation.

Figure 3.3.4: Phase contrast images of *SH-SY5Y* 2D cell cultures for morphological response of 25million cell/ml neuroblastoma cells incubated for 7 days with soluble form of NrCAM, NrCAM-GUVs, and 10-times lower concentration of NrCAM, NrCAM-GUVs. Retinoic acid was used in all cases to kick-start differentiation.

Figure 3.3.5: GAPDH normalized relative β-tubulin values

Figure 3.3.6: GAPDH normalized relative β-tubulin values values

Figure 3.3.7: GAPDH normalized relative β-tubulin values values

Figure 3.3.8: GAPDH normalized relative β-tubulin values values

- ## Tables:

Table 2.1.1: Table of chemicals

Table 2.1.2: Table of biologicals used in the experiments

Table 2.1.3: Table of cells used for the measurements

Table 2.1.4: Table of materials used in the experiments

Table 2.2.1: Basic GUV composite for creating concentration standard curve, 6000µM

Table 2.2.2: NTA containing GUV-s, 6000 µM

Table 2.2.3: Applied antibodies

Table 3.3.1: Effect of different concentration of retinoic acid on neuroblastoma (*SH-SY5Y*) cells on day 1-3-7 in 2D and 3D cultures.

Table 3.3.2: GAPDH normalized relative beta tubulin values. Red shows the values lower than the signal of the control sample.

List of abbreviations

2D- Two-dimensional

3D - Three dimensional

ALS - Amyotrophic Lateral Sclerosis

ATRA - All-*trans*-retinoic acid

BSA - Bovine serum albumin

CNC - Computer numerical control

CNS - Central nervous system

DMEM - Dulbecco's Modified Eagle Medium

DMSO - Dimethyl sulfoxide

dsGUV - Droplet stabilized giant unilamelar vesciles

FNIII - Fibronectin type III

GPI - Glycosylphosphatidylinositol

GUV - Giant unilamelar vesicles

HFE - Hydrofluoroether

Ig - Immunoglobulin

LDS - Lithium dodecyl sulfate

MOPS - (3-(N-morpholino)propanesulfonic acid)

NgCAM - Neuron-glia cell adhesion molecule

NrCAM - Neuron-glial related cell adhesion molecule

NSE - Neuron specific enolase

NTA - Nitrilotriacetic acid

PBS - Phosphate buffered saline

PDMS - Polydimethylsiloxane

PEG - Polyethylene glycol- Perfluorpolypropylene

PFA - Paraformaldehyde

PFPE - Perfluorpolypropylene

PMMA - Polymethylmethacrylat

PNS - Peripheral nervous system

RA - Retinoic acid

RCF - Relative centrifugal force

SUV - Small unilamelar vesicles

TBST - Tris-buffered saline - Tween 20

WGA - Wheat germ agglutinin

Bibliography

[1] J. Kovalevich and D. Langford, "Considerations for the use of SH-SY5Y neuroblastoma cells in neurobiology," in *Neuronal Cell Culture*Anonymous Springer, 2013, pp. 9-21.

[2] J. M. Maris and K. K. Matthay, "Molecular biology of neuroblastoma," *Journal of Clinical Oncology,* vol. 17, *(7),* pp. 2264, 1999.

[3] M. Encinas, M. Iglesias, Y. Liu, H. Wang, A. Muhaisen, V. Cena, C. Gallego and J. X. Comella, "Sequential treatment of SH-SY5Y cells with retinoic acid and brain-derived neurotrophic factor gives rise to fully differentiated, neurotrophic factor-dependent, human neuron-like cells," *J. Neurochem.,* vol. 75, *(3),* pp. 991-1003, 2000.

[4] J. I. Forster, S. Köglsberger, C. Trefois, O. Boyd, A. S. Baumuratov, L. Buck, R. Balling and P. Antony, "Characterization of differentiated SH-SY5Y as neuronal screening model reveals increased oxidative vulnerability," *Journal of Biomolecular Screening,* vol. 21, *(5),* pp. 496-509, 2016.

[5] H. Xicoy, B. Wieringa and G. J. Martens, "The SH-SY5Y cell line in Parkinson's disease research: a systematic review," *Molecular Neurodegeneration,* vol. 12, *(1),* pp. 10, 2017.

[6] L. Agholme, T. Lindström, K. Kågedal, J. Marcusson and M. Hallbeck, "An in vitro model for neuroscience: differentiation of SH-SY5Y cells into cells with morphological and biochemical characteristics of mature neurons," *J. Alzheimer's Dis.,* vol. 20, *(4),* pp. 1069-1082, 2010.

[7] M. M. Shipley, C. A. Mangold and M. L. Szpara, "Differentiation of the SH-SY5Y human neuroblastoma cell line," *JoVE (Journal of Visualized Experiments), (108),* pp. e53193, 2016.

[8] R. B. van Breemen, D. Nikolic, X. Xu, Y. Xiong, M. van Lieshout, C. E. West and A. B. Schilling, "Development of a method for quantitation of retinol and retinyl palmitate in human serum using high-performance liquid chromatography–atmospheric pressure chemical ionization–mass spectrometry," *Journal of Chromatography A,* vol. 794, *(1-2),* pp. 245-251, 1998.

[9] National Research Council (US). Committee on Biological Chemistry, *Specifications and Criteria for Biochemical Compounds.* National Academies, 1967*1344.*

[10] G. López-Carballo, L. Moreno, S. Masiá, P. Pérez and D. Barettino, "Activation of the phosphatidylinositol 3-kinase/Akt signaling pathway by retinoic acid is required for neural

differentiation of SH-SY5Y human neuroblastoma cells," *J. Biol. Chem.,* vol. 277, *(28),* pp. 25297-25304, 2002.

[11] H. Ben-Sasson, A. Ben-Meir, A. Shushan, L. Karra, N. Rojansky, B. Y. Klein, R. Levitzki and H. Ben-Bassat, "All-trans-retinoic acid mediates changes in PI3K and retinoic acid signaling proteins of leiomyomas," *Fertil. Steril.,* vol. 95, *(6),* pp. 2080-2086, 2011.

[12] Y. Cheung, W. K. Lau, M. Yu, C. S. Lai, S. Yeung, K. So and R. C. Chang, "Effects of all-trans-retinoic acid on human SH-SY5Y neuroblastoma as in vitro model in neurotoxicity research," *Neurotoxicology,* vol. 30, *(1),* pp. 127-135, 2009.

[13] D. Uberti, C. Rizzini, P. Spano and M. Memo, "Characterization of tau proteins in human neuroblastoma SH-SY5Y cell line," *Neurosci. Lett.,* vol. 235, *(3),* pp. 149-153, 1997.

[14] K. K. Matthay, J. G. Villablanca, R. C. Seeger, D. O. Stram, R. E. Harris, N. K. Ramsay, P. Swift, H. Shimada, C. T. Black and G. M. Brodeur, "Treatment of high-risk neuroblastoma with intensive chemotherapy, radiotherapy, autologous bone marrow transplantation, and 13-cis-retinoic acid," *N. Engl. J. Med.,* vol. 341, *(16),* pp. 1165-1173, 1999.

[15] P. F. Shen, "Molecular mechanisms of chemoprevention and therapy of cancer by retinoids," *Front. Biosci.,* vol. 9, pp. 2663-2670, 2004.

[16] M. V. Sofroniew and H. V. Vinters, "Astrocytes: biology and pathology," *Acta Neuropathol.,* vol. 119, *(1),* pp. 7-35, 2010.

[17] M. Nedergaard, B. Ransom and S. A. Goldman, "New roles for astrocytes: redefining the functional architecture of the brain," *Trends Neurosci.,* vol. 26, *(10),* pp. 523-530, 2003.

[18] A. C. Lepore, B. Rauck, C. Dejea, A. C. Pardo, M. S. Rao, J. D. Rothstein and N. J. Maragakis, "Focal transplantation–based astrocyte replacement is neuroprotective in a model of motor neuron disease," *Nat. Neurosci.,* vol. 11, *(11),* pp. 1294, 2008.

[19] L. Pellerin and P. J. Magistretti, "Neuroenergetics: calling upon astrocytes to satisfy hungry neurons," *Neuroscientist,* vol. 10, *(1),* pp. 53-62, 2004.

[20] W. Chung, N. J. Allen and C. Eroglu, "Astrocytes control synapse formation, function, and elimination," *Cold Spring Harbor Perspectives in Biology,* vol. 7, *(9),* pp. a020370, 2015.

[21] S. A. Sloan and B. A. Barres, "Mechanisms of astrocyte development and their contributions to neurodevelopmental disorders," *Curr. Opin. Neurobiol.,* vol. 27, pp. 75-81, 2014.

[22] M. R. Williams, T. Hampton, R. K. Pearce, S. R. Hirsch, O. Ansorge, M. Thom and M. Maier, "Astrocyte decrease in the subgenual cingulate and callosal genu in schizophrenia," *Eur. Arch. Psychiatry Clin. Neurosci.,* vol. 263, *(1),* pp. 41-52, 2013.

[23] D. Fitzli, E. T. Stoeckli, S. Kunz, K. Siribour, C. Rader, B. Kunz, S. V. Kozlov, A. Buchstaller, R. P. Lane and D. M. Suter, "A direct interaction of axonin-1 with NgCAM-related cell adhesion molecule (NrCAM) results in guidance, but not growth of commissural axons," *J. Cell Biol.,* vol. 149, *(4),* pp. 951-968, 2000.

[24] T. Shiga and R. W. Oppenheim, "Immunolocalization studies of putative guidance molecules used by axons and growth cones of intersegmental interneurons in the chick embryo spinal cord," *J. Comp. Neurol.,* vol. 310, *(2),* pp. 234-252, 1991.

[25] E. T. Stoeckli and L. T. Landmesser, "Axonin-1, Nr-CAM, and Ng-CAM play different roles in the in vivo guidance of chick commissural neurons," *Neuron,* vol. 14, *(6),* pp. 1165-1179, 1995.

[26] H. Kamiguchi and V. Lemmon, "Neural cell adhesion molecule L1: signaling pathways and growth cone motility," *J. Neurosci. Res.,* vol. 49, *(1),* pp. 1-8, 1997.

[27] G. Morales, M. Hubert, T. Brümmendorf, U. Treubert, A. Tárnok, U. Schwarz and F. G. Rathjen, "Induction of axonal growth by heterophilic interactions between the cell surface recognition proteins Fll and Nr-CAM/Bravo," *Neuron,* vol. 11, *(6),* pp. 1113-1122, 1993.

[28] M. Lustig, T. Sakurai and M. Grumet, "Nr-CAM promotes neurite outgrowth from peripheral ganglia by a mechanism involving axonin-1 as a neuronal receptor," *Dev. Biol.,* vol. 209, *(2),* pp. 340-351, 1999.

[29] T. Sakurai, "The role of NrCAM in neural development and disorders—beyond a simple glue in the brain," *Molecular and Cellular Neuroscience,* vol. 49, *(3),* pp. 351-363, 2012.

[30] D. M. Suter, G. E. Pollerberg, A. Buchstaller, R. J. Giger, W. J. Dreyer and P. Sonderegger, "Binding between the neural cell adhesion molecules axonin-1 and Nr-CAM/Bravo is involved in neuron-glia interaction." *J. Cell Biol.,* vol. 131, *(4),* pp. 1067-1081, 1995.

[31] L. R. Herron, M. Hill, F. Davey and F. J. Gunn-Moore, "The intracellular interactions of the L1 family of cell adhesion molecules," *Biochem. J.,* vol. 419, *(3),* pp. 519-531, 2009.

[32] L. Su, X. Song, H. Wei and H. Yin, "Identification of neuron-related genes for cell therapy of neurological disorders by network analysis," *Journal of Zhejiang University-SCIENCE B,* vol. 18, *(2),* pp. 172-182, 2017.

[33] K. Susuki, K. Chang, D. R. Zollinger, Y. Liu, Y. Ogawa, Y. Eshed-Eisenbach, M. T. Dours-Zimmermann, J. A. Oses-Prieto, A. L. Burlingame and C. I. Seidenbecher, "Three mechanisms assemble central nervous system nodes of Ranvier," *Neuron,* vol. 78, *(3),* pp. 469-482, 2013.

[34] D. Elias and H. J. Ditzel, "Fyn is an important molecule in cancer pathogenesis and drug resistance," *Pharmacological Research,* vol. 100, pp. 250-254, 2015.

[35] A. Buchstaller, S. Kunz, P. Berger, B. Kunz, U. Ziegler, C. Rader and P. Sonderegger, "Cell adhesion molecules NgCAM and axonin-1 form heterodimers in the neuronal membrane and cooperate in neurite outgrowth promotion." *J. Cell Biol.,* vol. 135, *(6),* pp. 1593-1607, 1996.

[36] M. Weiss, J. P. Frohnmayer, L. T. Benk, B. Haller, J. Janiesch, T. Heitkamp, M. Börsch, R. B. Lira, R. Dimova and R. Lipowsky, "Sequential bottom-up assembly of mechanically stabilized synthetic cells by microfluidics," *Nature Materials,* vol. 17, *(1),* pp. 89, 2018.

[37] J. Wilson and T. Hunt, *Molecular Biology of the Cell: The Problems Book.* Garland Science, 2014.

[38] B. Haller, K. Göpfrich, M. Schröter, J. Janiesch, I. Platzman and J. P. Spatz, "Charge controlled microfluidic formation of lipid-based single-and multicompartment systems," *Lab on a Chip,* 2018.

[39] Y. Ding, F. Wu and C. Tan, "Synthetic biology: A bridge between artificial and natural cells," *Life,* vol. 4, *(4),* pp. 1092-1116, 2014.

[40] E. Van der Pol, A. N. Böing, P. Harrison, A. Sturk and R. Nieuwland, "Classification, functions, and clinical relevance of extracellular vesicles," *Pharmacol. Rev.,* vol. 64, *(3),* pp. 676-705, 2012.

[41] I. Platzman, J. Janiesch and J. P. Spatz, "Synthesis of nanostructured and biofunctionalized water-in-oil droplets as tools for homing T cells," *J. Am. Chem. Soc.,* vol. 135, *(9),* pp. 3339-3342, 2013.

[42] J. Song, Q. Ye, W. T. Lee, X. Wang, T. He, K. W. Shah and J. Xu, "Perfluoropolyether/poly (ethylene glycol) triblock copolymers with controllable self-assembly behaviour for highly efficient anti-bacterial materials," *RSC Advances,* vol. 5, *(79),* pp. 64170-64179, 2015.

[43] K. Göpfrich, B. Haller, O. Staufer, Y. Dreher, U. Mersdorf, I. Platzman and J. P. Spatz, "One-Pot Assembly of Complex Giant Unilamellar Vesicle-Based Synthetic Cells," *ACS Synthetic Biology,* 2019.

[44] W. C. Hahn, C. M. Counter, A. S. Lundberg, R. L. Beijersbergen, M. W. Brooks and R. A. Weinberg, "Creation of human tumour cells with defined genetic elements," *Nature,* vol. 400, *(6743),* pp. 464, 1999.

[45] H. Dolznig, C. Rupp, C. Puri, C. Haslinger, N. Schweifer, E. Wieser, D. Kerjaschki and P. Garin-Chesa, "Modeling colon adenocarcinomas in vitro: A 3D co-culture system induces cancer-relevant pathways upon tumor cell and stromal fibroblast interaction," *The American Journal of Pathology,* vol. 179, *(1),* pp. 487-501, 2011.

[46] A. Riedl, M. Schlederer, K. Pudelko, M. Stadler, S. Walter, D. Unterleuthner, C. Unger, N. Kramer, M. Hengstschläger and L. Kenner, "Comparison of cancer cells in 2D vs 3D culture reveals differences in AKT–mTOR–S6K signaling and drug responses," *J. Cell. Sci.,* vol. 130, *(1),* pp. 203-218, 2017.

[47] I. Kelava and M. A. Lancaster, "Dishing out mini-brains: current progress and future prospects in brain organoid research," *Dev. Biol.,* vol. 420, *(2),* pp. 199-209, 2016.

[48] M. A. Lancaster, M. Renner, C. Martin, D. Wenzel, L. S. Bicknell, M. E. Hurles, T. Homfray, J. M. Penninger, A. P. Jackson and J. A. Knoblich, "Cerebral organoids model human brain development and microcephaly," *Nature,* vol. 501, *(7467),* pp. 373, 2013.

[49] G. Rossi, A. Manfrin and M. P. Lutolf, "Progress and potential in organoid research," *Nature Reviews Genetics,* pp. 1, 2018.

[50] B. S. Freedman, C. R. Brooks, A. Q. Lam, H. Fu, R. Morizane, V. Agrawal, A. F. Saad, M. K. Li, M. R. Hughes and R. Vander Werff, "Modelling kidney disease with CRISPR-mutant kidney organoids derived from human pluripotent epiblast spheroids," *Nature Communications,* vol. 6, pp. 8715, 2015.

[51] F. Pampaloni, N. Ansari and E. H. Stelzer, "High-resolution deep imaging of live cellular spheroids with light-sheet-based fluorescence microscopy," *Cell Tissue Res.,* vol. 352, *(1),* pp. 161-177, 2013.

[52] R. C. Bates, N. S. Edwards and J. D. Yates, "Spheroids and cell survival," *Crit. Rev. Oncol.,* vol. 36, *(2-3),* pp. 61-74, 2000.

[53] A. Takagi, M. Watanabe, Y. Ishii, J. Morita, Y. Hirokawa, T. Matsuzaki and T. Shiraishi, "Three-dimensional cellular spheroid formation provides human prostate tumor cells with tissue-like features," *Anticancer Res.,* vol. 27, *(1A),* pp. 45-53, 2007.

[54] B. Desoize and J. Jardillier, "Multicellular resistance: a paradigm for clinical resistance?" *Crit. Rev. Oncol.,* vol. 36, *(2-3),* pp. 193-207, 2000.

[55] B. Kwak, Y. Lee, J. Lee, S. Lee and J. Lim, "Mass fabrication of uniform sized 3D tumor spheroid using high-throughput microfluidic system," *J. Controlled Release,* vol. 275, pp. 201-207, 2018.

[56] L. Goers, P. Freemont and K. M. Polizzi, "Co-culture systems and technologies: taking synthetic biology to the next level," *Journal of the Royal Society Interface,* vol. 11, *(96),* pp. 20140065, 2014.

[57] G. Piret, M. Perez and C. N. Prinz, "Support of neuronal growth over glial growth and guidance of optic nerve axons by vertical nanowire arrays," *ACS Applied Materials & Interfaces,* vol. 7, *(34),* pp. 18944-18948, 2015.

[58] M. Shi, D. Majumdar, Y. Gao, B. M. Brewer, C. R. Goodwin, J. A. McLean, D. Li and D. J. Webb, "Glia co-culture with neurons in microfluidic platforms promotes the formation and stabilization of synaptic contacts," *Lab on a Chip,* vol. 13, *(15),* pp. 3008-3021, 2013.

[59] T. Achilli, J. Meyer and J. R. Morgan, "Advances in the formation, use and understanding of multi-cellular spheroids," *Expert Opinion on Biological Therapy,* vol. 12, *(10),* pp. 1347-1360, 2012.

[60] M. Chen, M. P. Shah, T. B. Shelper, L. Nazareth, M. Barker, J. Tello Velasquez, J. A. Ekberg, M. Vial and J. St John, "Naked liquid marbles: a robust three-dimensional low-volume cell culturing system," *ACS Applied Materials & Interfaces,* 2019.

[61] P. Sabhachandani, V. Motwani, N. Cohen, S. Sarkar, V. Torchilin and T. Konry, "Generation and functional assessment of 3D multicellular spheroids in droplet based microfluidics platform," *Lab on a Chip,* vol. 16, *(3),* pp. 497-505, 2016.

[62] H. Gu, M. H. Duits and F. Mugele, "Droplets formation and merging in two-phase flow microfluidics," *International Journal of Molecular Sciences,* vol. 12, *(4),* pp. 2572-2597, 2011.

[63] X. Zhao, Y. Xia and G. M. Whitesides, "Fabrication of three-dimensional micro-structures: Microtransfer molding," *Adv Mater,* vol. 8, *(10),* pp. 837-840, 1996.

[64] L. Xiong, P. Chen and Q. Zhou, "Adhesion promotion between PDMS and glass by oxygen plasma pre-treatment," *J. Adhes. Sci. Technol.,* vol. 28, *(11),* pp. 1046-1054, 2014.

[65] M. Pekker and M. N. Shneider, "The surface charge of a cell lipid membrane," *arXiv Preprint arXiv:1401.4707,* 2014.

[66] K. Webb, V. Hlady and P. A. Tresco, "Relative importance of surface wettability and charged functional groups on NIH 3T3 fibroblast attachment, spreading, and cytoskeletal organization," *Journal of Biomedical Materials Research: An Official Journal of the Society for Biomaterials, the Japanese Society for Biomaterials, and the Australian Society for Biomaterials,* vol. 41, *(3),* pp. 422-430, 1998.

[67] C. X. Guo, X. T. Zheng, S. R. Ng, Y. Lai, Y. Lei and C. M. Li, "In situ molecular detection of ischemic cells by enhanced protein direct electron transfer on a unique

horseradish peroxidase–Au nanoparticles–polyaniline nanowires biofilm," *Chemical Communications,* vol. 47, *(9),* pp. 2652-2654, 2011.

[68] S. C. Baicu and M. J. Taylor, "Acid–base buffering in organ preservation solutions as a function of temperature: new parameters for comparing buffer capacity and efficiency," *Cryobiology,* vol. 45, *(1),* pp. 33-48, 2002.

[69] Y. Xia and G. M. Whitesides, "Soft lithography," *Annual Review of Materials Science,* vol. 28, *(1),* pp. 153-184, 1998.

[70] T. W. Hofmann, S. Hänselmann, J. Janiesch, A. Rademacher and C. H. Böhm, "Applying microdroplets as sensors for label-free detection of chemical reactions," *Lab on a Chip,* vol. 12, *(5),* pp. 916-922, 2012.

[71] D. Semwogerere and E. R. Weeks, "Confocal microscopy," *Encyclopedia of Biomaterials and Biomedical Engineering,* vol. 23, pp. 1-10, 2005.

[72] J. Pawley, *Handbook of Biological Confocal Microscopy.* Springer Science & Business Media, 2010.

[73] R. Wegerhoff, O. Weidlich and M. Kassens, "Basics of light microscopy and imaging," *Imaging & Microscopy,* pp. 1-56, 2007.

[74] A. Alegria-Schaffer, A. Lodge and K. Vattem, "Performing and optimizing western blots with an emphasis on chemiluminescent detection," in *Methods in Enzymology*Anonymous Elsevier, 2009, pp. 573-599.

[75] Z. Castaño and R. M. Kypta, "Housekeeping proteins: limitations as references during neuronal differentiation," *Open Neurosci J,* vol. 2, *(1),* pp. 36-40, 2008.